CHALMERS
UNIVERSITY OF TECHNOLOGY

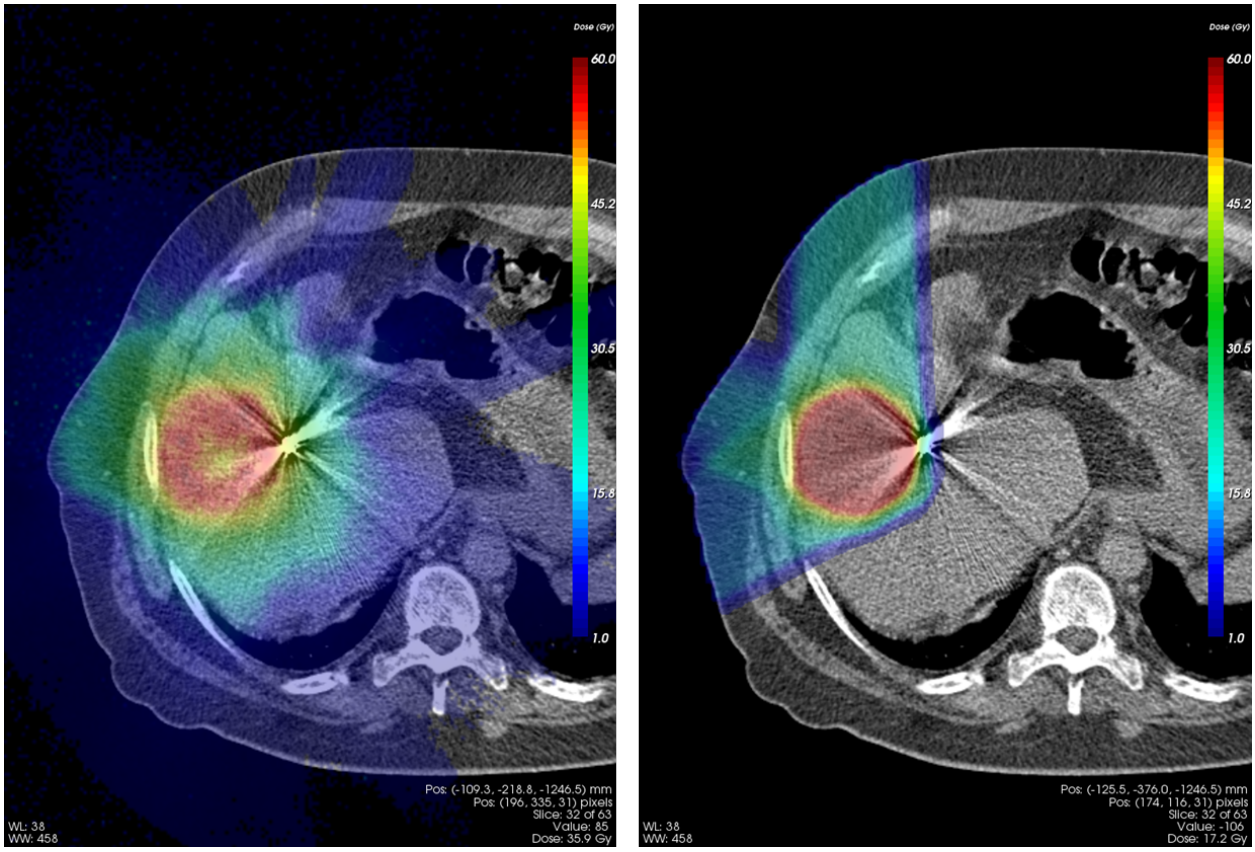

Intensity Modulated Proton Therapy for Hepatocellular Carcinoma

A Simulation Study of the Interplay Effect for Comparison with Photon Therapy

Master's thesis in Biomedical Engineering

Lovisa Westlund Gotby

Department of Physics
CHALMERS UNIVERSITY OF TECHNOLOGY
Gothenburg, Sweden 2017

Master's thesis

Intensity Modulated Proton Therapy for Hepatocellular Carcinoma

A Simulation Study of the Interplay Effect for Comparison with Photon Therapy

LOVISA WESTLUND GOTBY

CHALMERS
UNIVERSITY OF TECHNOLOGY

Department of Physics
Division of Subatomic and Plasma Physics
Chalmers University of Technology
Gothenburg, Sweden 2017

Intensity Modulated Proton Therapy for Hepatocellular Carcinoma
A Simulation Study of the Interplay Effect for Comparison with Photon Therapy
LOVISA WESTLUND GOTBY

Supervisor: Petra Trnkova, Holland Particle Therapy Centre
Examiner: Anders Nordlund, Department of Physics

Master's Thesis CTH-NT-328
ISSN 1653-4662
Department of Physics
Division of Subatomic and Plasma Physics
Chalmers University of Technology
SE-412 96 Gothenburg
Telephone +46 31 772 1000

Cover: Dose distributions on in the transverse plane of the abdomen. The left image shows a photon SBRT dose distribution and the right image shows a dose distribution from an IMPT plan.

Typeset in LaTeX
Gothenburg, Sweden 2017

Intensity Modulated Proton Therapy for Hepatocellular Carcinoma
A Simulation Study of the Interplay Effect for Comparison with Photon Therapy
LOVISA WESTLUND GOTBY
Department of Physics
Chalmers University of Technology

Abstract

This is a preliminary study investigating the advantages and drawbacks of using intensity modulated proton therapy (IMPT) in the treatment of hepatocellular carcinoma (HCC) and compares this treatment modality with photon stereotactic body radiation therapy (SBRT). One patient, previously treated with photon SBRT, has been replanned and by benefiting from the protons finite range and the fact that most of the dose is deposited in the Bragg peak, proton treatment plans which efficiently spare the organs-at-risk (OARs) have been generated. The challenge with using IMPT when treating HCC however, is that the tumor moves over time due to breathing and the sensitive spatio-temporal resolution of the IMPT is therefore compromised in the treatment delivery, giving rise to the so-called interplay effect. This effect can be mitigated by, for example, breath hold, beam gating, tumor tracking or rescanning.

The impact of interplay effect has been simulated for treatment delivery in breath hold as well as for free-breathing and the benefit of using rescanning has been investigated. All IMPT plans have superior tumor coverage in comparison with the photon SBRT plan, at the same time as having better OAR sparing. The dose delivery simulations show promising results for future clinical applications of robust proton therapy treatment plans for both delivery techniques, the trade-off between dose delivery in breath hold and free-breathing being treatment time versus sparing of OARs. However, more patient cases are needed in order to draw more general conclusions.

Keywords: IMPT, SBRT, HCC, 4DCT, interplay effect, robust planning

Acknowledgements

First I would like to thank the whole medical physics group at the Erasmus Medical Center Cancer Institute for giving me a warm and friendly welcome to the department and for always reaching out a helping hand. A special thanks goes out to my supervisor Petra Trnkova, medical physicist at the Holland Particle Therapy Center, and Mischa Hoogeman, Head of Medical Physics at the Erasmus Medical Center Cancer Institute, for giving me the opportunity to carry out this project and for pushing the work forward by asking thoughtful and challenging questions for me to answer. I would also like to thank Alejandra Méndez Romero, radiation oncologist at the Erasmus Medical Center Cancer Institute, for the giving clinical insight into the problem which this thesis aims to investigate. A huge thanks also to Thyrza Jagt, PhD canditate at the Erasmus Medical Center Cancer Institute, for tireless help with the simulation tools and to Dominique Reijtenbagh, master's thesis student of the TU Delft, for all the moral support.

Lastly, I would like to thank Edwin Versteeg for being by my side and continuously pushing me do better even when I have doubts. Without you, I would not have realized this project.

Lovisa Westlund Gotby, Gothenburg, June 2017

Contents

1
Introduction

This thesis investigates the prospects of using intensity modulated proton therapy (IMPT) for the treatment of, the liver based cancer, hepatocellular carcinoma (HCC). The benefits and drawbacks of the IMPT treatment in comparison to stereotactic body radiation therapy (SBRT) with photons will also be investigated.

1.1 Background

HCC is one of the most commonly occurring types of cancers worldwide, with a high risk of fatal outcome for the affected patient [1]. HCC is mostly preceded by an infection or other long term damage to the liver and, due to this, the tolerance towards irradiation of the liver tissue, surrounding the tumor, is therefore decreased and the risk of toxicity is increased. In radiation therapy, there is always a trade-off between tumor control and induced toxicity to the healthy tissue, such as the normal liver, with the goal always being to give a precise, conformal and high dose to the target while sparing the organs at risk (OARs) [2].

The treatment with photon SBRT fulfills the requirement of being precise, conformal and able to deliver a high target dose, but lacks on the point of being able to spare the OARs sufficiently, this due to the intrinsic physical properties of photons interacting with tissue. Because of this dose delivered to the healthy tissue, the use of photon SBRT in treatment of HCC is consequently not optimal. A good alternative to photon SBRT is IMPT which would offer better sparing of, i.e. lower doses to, the surrounding tissue. Protons have the property of finite range, which is dependant on their initial energy, meaning that they at some point will stop in the tissue and not deliver any more dose. A considerable part of the delivered dose is localized at the end of the range of the proton, in the so-called Bragg peak [1], and this quality of the protons is exactly what makes them favourable over photons.

With the Bragg peak being very localized, however, the dose delivery is sensitive to uncertainties and it needs to be steered and applied in multiple spots in order to create a conformal dose distribution to the target volume. To cover the entire volume, the proton beam is magnetically deflected in order to deliver spots in a plane and the energies of the protons are varied to change the tissue depth. The uncertainties in the dose delivery are dependent on the range of the protons, setup errors of the patient and internal organ movements. It is of utmost importance to take all these uncertainties into account in order to generate a high quality treatment plan which is also safe to deliver. The liver is being situated right underneath the diaphragm, which controls the breathing, and is therefore moving with every respiratory cycle. If no regard is taken to the respiratory motion in the treatment planning and delivery, this can lead to an under-dosage of the target volume and an over-dosage of the surrounding tissue, the so-called interplay effect.

1.2 Aim

This project aims to examine how to develop clinically relevant IMPT treatment plans which are based on the SBRT irradiation technique and are specialized for treatment of HCC. The goal is that the IMPT plans should have similar or better quality than the already existing photon SBRT treatment plans. The main focus will be to simulate treatment delivery in both 3D and 4D perspectives while taking relevant uncertainties and changes of anatomy into account. Four different approaches, will be considered in order to achieve the final goal with this project. These are described as follows;

- 3D non-robust IMPT treatment plan which allows dose escalation to the target in order to spare surrounding tissue, this means that the delivered target dose can be inhomogeneous and that some parts of the target can receive a dose which is significantly higher than the prescribed one.
- 3D robust IMPT treatment plan, uncertainties regarding proton range and patient setup errors are considered.
- 4D non-robust IMPT treatment plan taking multiple breathing phases into account in the planning.
- 4D robust IMPT treatment plan taking both uncertainties regarding proton range and patient setup errors into account as well as motion of the target.

Notice that a 3D treatment plan is the equivalent of treating the patient during breath hold or respiratory compression and that a 4D treatment plan is delivered during free-breathing. These IMPT plans will be internally evaluated and their benefits and drawbacks, compared to today's photon SBRT treatment plans, will be assessed.

1.3 Limitations

This thesis project, which has to be carried out within the time span of 20 weeks, has been limited to only investigate one patient case. The reason for this is both the low availability of representative patient data with high enough quality to allow for 4D planning, and because time limitations due to calculation time of the treatment planning and simulation delivery. The project has been carried out at the Erasmus Medical Center Cancer Institute in Rotterdam, the Netherlands.

2
Theory

This chapter will describe all the background theory needed in order to get a good understanding of the problem at hand and the tools which can be used for finding a solution to this problem. It will also provide a good basis interpreting the results and the following conclusions.

2.1 The liver and HCC

The liver is the largest gland in the body making up about 2% of the total mass of an average sized adult [3]. Being positioned directly underneath the diaphragm, it is occupying most of the right upper quadrant of the abdomen and the stomach, gallbladder, pancreas and intestine are located in its absolute proximity, see Figure 2.1. Due to its position, the liver moves during breathing when the diaphragm alternates between contracting and relaxing. This movement of the liver is most prevalent in the superior-inferior direction where it ranges between 5 to 50 mm [4]. The liver performs a variety of metabolic and regulatory tasks in the body, for example creating bile for the digestive system and filtering out nutrients and waste material from the blood [3], and it is hence very important for the daily function of the human body.

The liver is a regenerative and parallel functioning organ [5], meaning that it has the capacity to recover and even regrow after it has been damaged or partially removed. This ability is however highly dependent of the condition of the liver and the volume which has not been damaged or is still left. To be able to regain as much functionality of the liver as possible after damage or resection, it is therefore important to always try to spare the healthy parts of the liver.

Hepatocellular carcinoma (HCC) is a primary liver cancer which is most often preceded by long-time damage to the liver, leading to cirrhosis, or by infection, such as Hepatitis B or Hepatitis C [1]. Both cirrhosis and infection are main risk factors for this type of cancer and it is advisable to employ screening programs for the population in this risk group since an early diagnosis provides a much better prognosis for the exposed patient. The best treatments against HCC, considering the long-term survival of the patient, are surgical resection of the tumor or a full liver transplant [1]. However, less than 30% of the HCC patients are eligible for these kinds of highly invasive surgeries [6]. This is, among other things, because it is difficult to find matching donor organs, because the tumor simply is not resectable or because the patient is very weak and this compromises the recovery from a cumbersome surgery.

Other treatments for HCC are radiofrequency ablation, transarterial chemoemolization, alcohol injection, cryotherapy and focused ultrasound therapy [1, 2]. Many patients, which are ineligible for surgical resection and transplantation, are however often also ineligible for these other treatments, and their use is therefore very limited. External beam irradiation therapy has been an established method in treatment of HCC for over

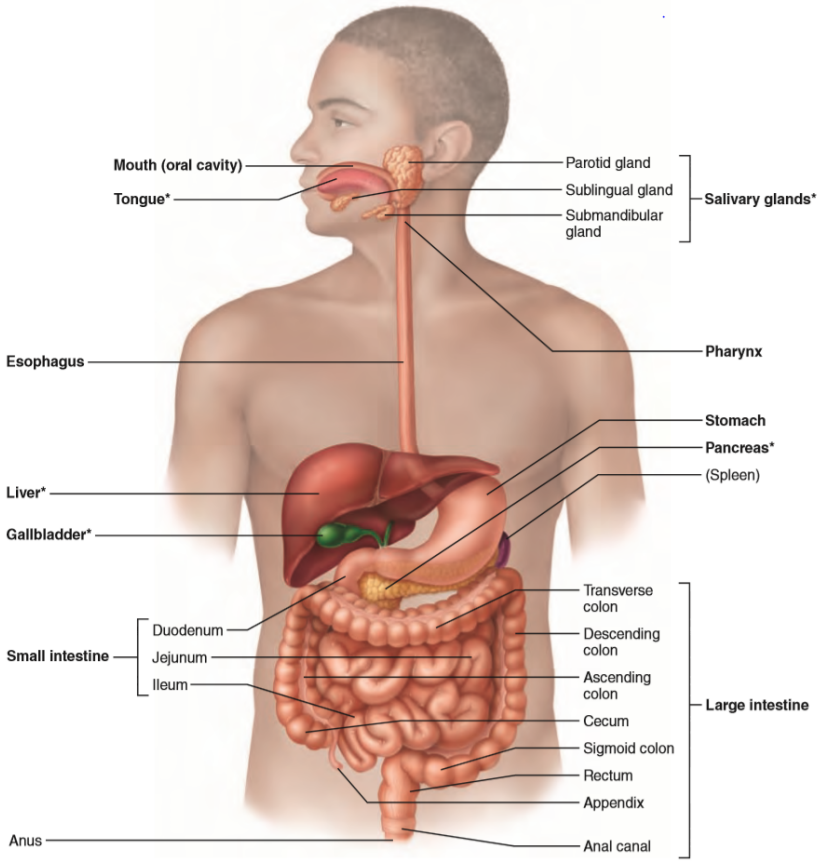

Figure 2.1: Gross anatomy of the full digestive system in which the liver plays an important roll. The image has been adapted from [3].

a decade [7], and it remains the best option for patients who can not be treated with another technique. It has the benefit of being non-invasive, and since the introduction of stereotactic body radiation therapy (SBRT) with photons, a high and conformal radiation dose can be deliver to the tumor. The drawback with photon SBRT is that also the healthy tissues surrounding the tumor receive a fairly high dose. As aforementioned, the liver in patients with HCC is often exposed to cirrhosis, which makes the liver more radiosensitive, and it is thereby easier to induce undesired toxicity in this tissue [2]. Another non-invasive treatment which has much better healthy tissue sparing than photon SBRT is intensity modulated proton therapy (IMPT). A conventional method for the use of IMPT for moving targets such as the liver is yet to be established however, and more research is therefore needed in this area.

2.2 External beam radiotherapy

In external beam radiotherapy, a beam of ionizing radiation is directed towards a patient with the aim of irradiating cancerous cells. The objective is to deliver a high enough radiation dose to induce cell death in the malignant cells, but at the same time sparing the surrounding healthy tissue and the organs at risk (OARs) in order to avoid radiation induced complications. Radiation therapy is a localized treatment and sparing of OARs is done by prescribing dose limits and plan treatments which meet the prescribed constraints. The total dose is delivered in one or more fractions. Fractionation of the dose means that

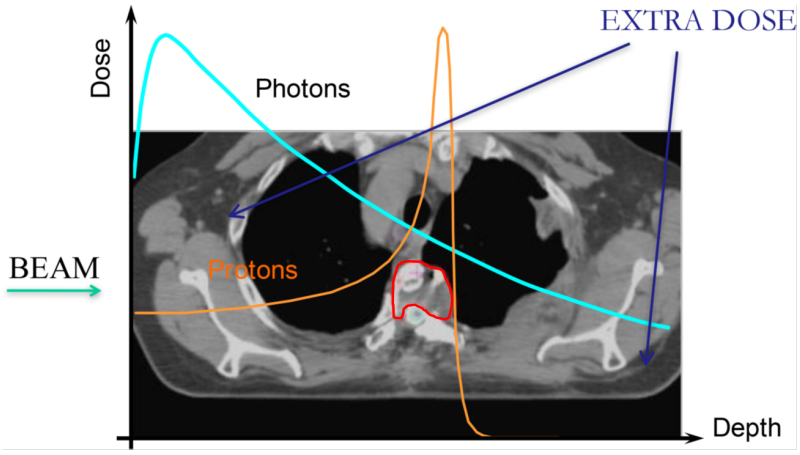

Figure 2.2: Illustration of the characteristics of the dose deposition curves for beams of mono-energetic photons (blue) and protons (orange), respectively. The photon beam deliver a dose to the tissue with exponentially decreasing intensity while most of the dose from the proton beam is localized in the Bragg peak which can be modulated to overlap with the target (red). The figure has been adapted from [8].

the total dose is divided into smaller parts which are delivered to the patient at separate occasions. The time between two different fractions can range from a couple of hours up to a few days. Cancer cells are generally more sensitive towards radiation than healthy tissue and do not possess the same ability of repairing themselves after receiving a dose. The advantage of fractionation is hence that the healthy tissue is given some time to recover, this without compromising the tumor control.

The most widely used external beam radiotherapy technique irradiates the target using photons with energy in the order of mega-electronvolts [8]. Other possibilities for choice of ionizing radiation are electrons, neutrons, alpha particles, protons or other heavy ions. As it can be seen in Figure 2.2, the dose deposition curves depending on tissue depth, for photons and protons, are intrinsically different. Photons are uncharged particles, meaning that they are indirectly ionizing and interact with matter by means of photo electric effect, Compton scattering or pair production, depending on the energy of the photons and the atomic number of the matter [9]. This leads to the fact that the photon beam is attenuated exponentially, continuously delivering dose to the tissue with decreasing intensity. Notice that photon beam fully penetrates the patient in Figure 2.2, and hence gives an exit dose. Protons, on the other hand, are charged particles and therefore directly ionizing. These particles have finite range and the energy they deposit is transferred to the tissue via electromagnetic interactions. The dose deposition is inversely proportional to their velocity, which leads to the maximum dose being delivered in the "Bragg peak" near the end of range for these particles [8].

The optimal scenario in radiotherapy is that all dose is delivered to the target, completely sparing the healthy tissue and the OARs. In reality however, this is not the case both because the treatment plan has to take uncertainties into account and because of the characteristics of the ionizing radiation. Comparing the dose deposition curves for the photon and the proton beam in Figure 2.2, one can see that a significant excessive dose is delivered to the patient when using photons instead of protons and that protons therefore are favourable because of their superior normal tissue sparing. Notice that the depth of the ionizing radiation depends on the initial energy, increasing the energy would mean that the curves in Figure 2.2 are shifted to the right.

2.2.1 Dose

The primary used quantity for measuring radiation is the absorbed dose, which most often simply is referred to as dose. This quantity is defined as an absorption of energy per unit mass (J/kg) and the unit for this measure is called gray (Gy) [10]. The absorbed dose can be used to describe irradiation of any target by any ionizing radiation. Different types of ionizing radiation does however deposit energy in material at different rates, protons having higher linear energy transfer (LET) than photons. This leads to a change in the biological effectiveness of one ionizing radiation compared to another. The value of the relative biological effectiveness (RBE) of protons versus photons, is commonly accepted to be 1.1 [11], meaning that a proton beam damages cells more efficiently than a photon beam and it implies that a lower dose can be used when treating tumors with protons instead of with photons without compromising the tumor control.

Recent studies of this area have however suggested that LET and RBE for protons cannot be described by static numbers, and that they would vary with the dose rate, the tissue type and with depth along the beam [12, 13]. This would make proton therapy planning more complex since models for this have to be incorporated in treatment planning systems. Nevertheless, for the sake of a direct and easy comparison between the photon and the proton plans in this report only the values of absorbed doses will be taken into account.

2.2.2 Photon SBRT

Stereotactic body radiation therapy (SBRT), utilizing intensity modulated photons, is a subdivision of external beam radiotherapy. The definition of photon SBRT is that it is a method of accurately delivering a conformal and high irradiation dose, in one or a few fractions, to an extracranial target [14]. This treatment can be delivered to the patient using a conventional linear accelerator, the more sophisticated volumetric arc therapy (VMAT) or with a fully robotic system. More degrees of freedom, for the treatment delivery, are introduced with higher complexity in the choice of machine. An advantage of increasing the complexity of the treatment delivery is that there are greater potential in terms of OAR sparing, but the downside is that the planning time increases and that there also is possible elongation of the treatment delivery time.

A requirement for a system being able to deliver a photon SBRT treatment is that the treatment facility has some kind of image-guidance or tumor tracking. Both the spatial resolution and temporal resolution of the target, in this visualization, has to be high enough for the dose to be delivered in a precise way based on the daily anatomy of a specific fraction and the possible intrafractional movement of the tumor.

2.2.3 IMPT

Intensity modulated proton therapy (IMPT) is an application of active scanning proton therapy utilizing pencil beams. During the treatment, the dose is “painted” on the target spot by spot, and hence Bragg peak by Bragg peak, for the whole volume. Every pencil beam has a Gaussian-shaped dose distribution, orthogonal to the beam direction, and the width of each beam varies with the initial energy of the protons, the depth in the tissue and the treatment delivery system [8]. When scanning, the beam is deflected in the plane orthogonal to the beam direction using magnets which are placed on the beam delivery nozzle and the protons tissue depth is controlled by changing the beam energy.

In IMPT, all fields delivered to the patient are optimized simultaneously in the treatment planning. That means that the field from each beam separately is allowed to deliver

an inhomogeneous dose to the target with steep in-field dose gradients, but with the goal that the cumulative dose from all the beams will still be homogeneous. This phenomenon is illustrated in Figure 2.3. The main advantage, of allowing for these heterogeneities in the separate fields, is that a smart treatment planning system has the possibility of sparing the OARs in a very efficient way and the main disadvantage is that a deviation in one of more of the fields will mess up the homogeneity of the cumulative dose more than if every field delivered a uniform dose.

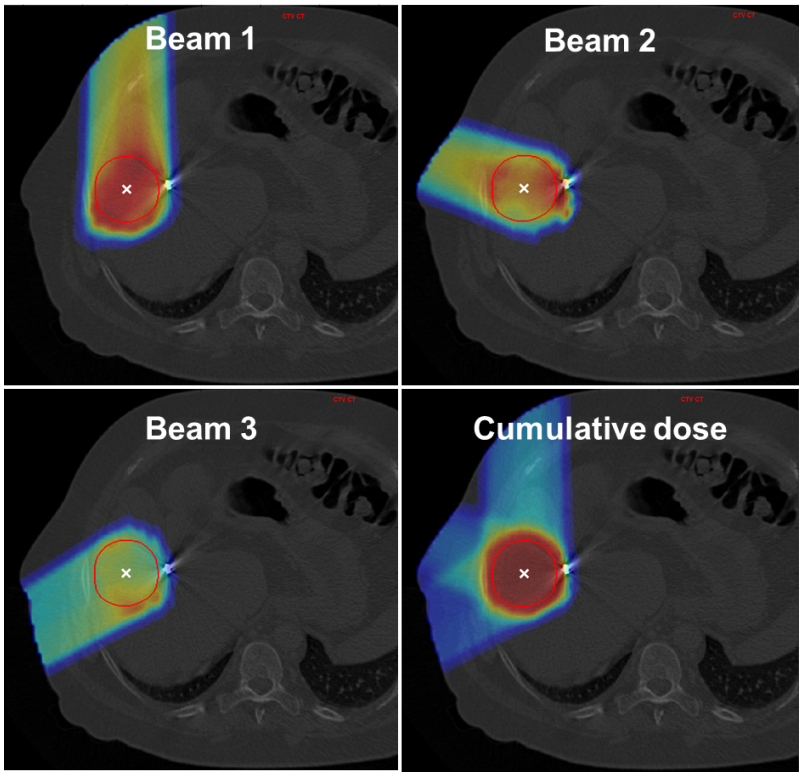

Figure 2.3: Separate contribution of the beams used in an IMPT treatment plan. Notice that each field is allowed to be inhomogeneous with steep dose gradients, but that the summation of all three fields together would yield a homogeneous coverage of the target (red).

2.3 Treatment planning

For the successful treatment of a tumor, not only the treatment delivery but also the treatment planning plays an important role. For this purpose, the aid of medical imaging is crucial and a three-dimensional planning computed tomography (CT) is obtained and contoured by a radiation oncologist. A full 3DCT set is composed of cross-sectional slices, in the axial plane, which are interpolated in the superior-inferior direction in order to create a volumetric image of the anatomy. Every slice in the CT is obtained by combining multiple X-ray images, taken from different angles during a rotation about the body, using a backprojection algorithm. X-rays are a type of ionizing radiation, meaning that the patient gets a dose while being scanned.

The contours on the planning CT are meant to separate the target from the OARs, so that dose constraints and limits can be prescribed. The three main structures which are usually contoured for the target are visualized in Figure 2.4. The gross tumor volume

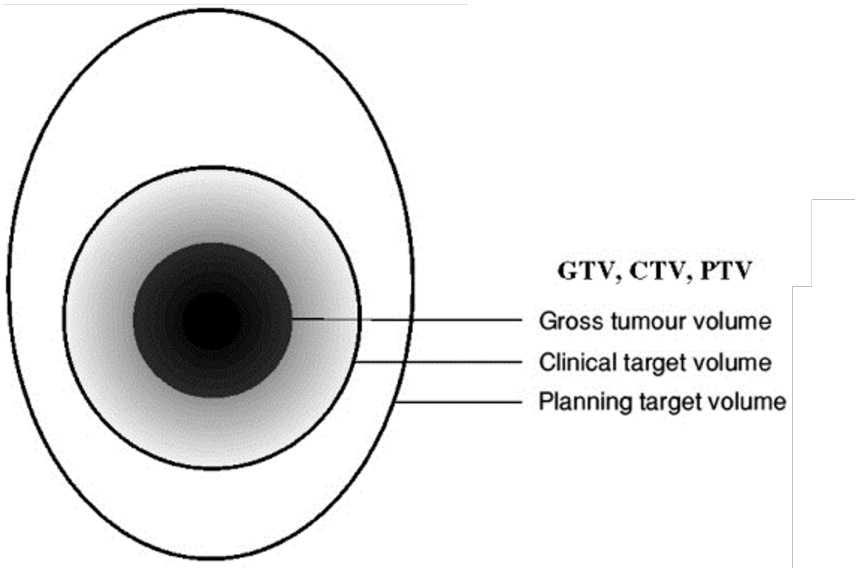

Figure 2.4: Graphical explanation of how target volumes are assigned for treatment planning in radiotherapy [16], these are the gross tumor volume (GTV), the clinical target volume (CTV) and the planning target volume (PTV).

(GTV) is defined as the outline of the visible malignant growth present on the CT image [15]. The clinical target volume (CTV) comprises the GTV and is meant to encompass any sub-clinical microscopic extensions of the malignant disease which can not be imaged with high enough resolution [9]. Some treatment planning protocols use a fixed margin, such as 1 cm, between the GTV and the CTV and other protocols, like the one used in this project for HCC, applies no margin between the GTV and the CTV. The third and last structure is the planning target volume (PTV). The PTV is a geometrical concept and is an extension of the CTV by some margin [15], which can be different in different directions as can be seen in Figure 2.4. In this project, an expansion of 5 mm between the CTV and PTV was used.

Furthermore, a four-dimensional computed tomography (4DCT) dataset is acquired for patients with mobile tumors in order to get an estimation of the range of the tumor motion. The fourth dimension in this scanning procedure refers to a time dependence of the anatomy, this dependency is based on the cyclic pattern of the lungs inflating and deflating during regular breathing. A 4DCT scan is obtained during free-breathing and after the scan, each CT slice acquired during the scanning procedure is binned to its respective breathing phase based on an independent measurement of the lung volume using an external marker. The resulting data from a 4DCT scan is one full 3DCT scan corresponding to each breathing phase. For 4D treatment planning to be possible, the full 4DCT dataset has to be contoured.

2.3.1 Uncertainties

There are always uncertainties in the delivery of radiotherapy which means that the delivered dose distribution will not totally correspond with the planned dose distribution. Such uncertainties are for example patient setup errors, interfractional motion, intrafractional motion and image artifacts in the planning CT. In order to generate a deliverable treatment plan that ensures a satisfying target coverage, these uncertainties have to be taken into account.

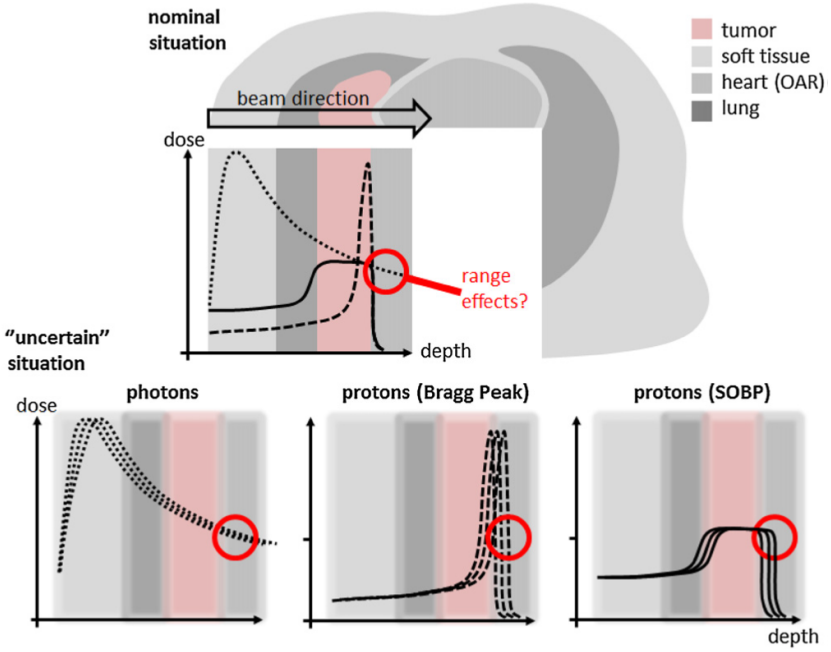

Figure 2.5: Illustration of the impact of range uncertainties in radiotherapy utilizing photons and protons, respectively. An overshoot or undershoot with photons only introduces a small difference in the dose to the OAR but a large difference in the case when protons are used instead. Both the mono-energetic proton beam and the modulated spread-out Bragg peak (SOBP) shows this sensitivity to range errors. The figure has been adapted from [17].

In photon radiotherapy, the PTV is meant to serve as an assurance that the dose prescribed to the CTV actually is delivered to the CTV. This margin should account for setup uncertainties, differences due to machine variations and intrafractional movement [15]. The concept of a geometrical approach, such as the PTV, is valid for photon therapy since the photon beam has a shallow dose fall-off, see Figure 2.2, and constraints on the dose to the PTV can therefore be prescribed.

In intensity modulated pencil beam scanning proton therapy however, a high dose (located in the Bragg peak) is delivered spot-wise to the target. As mentioned before, this characteristic is very advantageous in terms of OAR sparing but it also makes the treatment delivery very sensitive towards uncertainties. The PTV concept is not applicable here since a geometrical extension of the target does not always assure coverage in case of, for example, misalignment of fields with steep dose gradients [18]. Such a case could lead to loss of dose conformity in the middle of the target volume itself, which in other words means under- or over-dosage of the tumor. Another uncertainty which would cause a disagreement between the planned and the delivered dose distribution is range error of the protons. Exploiting the proton characteristic of finite range, a range uncertainty can lead to an over-dosage of an OAR, this is illustrated in Figure 2.5. In this figure one can see that a small range error for photon radiotherapy only yield a small difference in dose for the OAR in the disturbed scenario in comparison with the nominal situation. For IMPT however, the range uncertainty introduces a dose to the OAR which was not there in the nominal case, and furthermore, this uncertainty also introduces a risk of missing a part of the target.

So how to deal with uncertainties in treatment planning in IMPT? The answer to

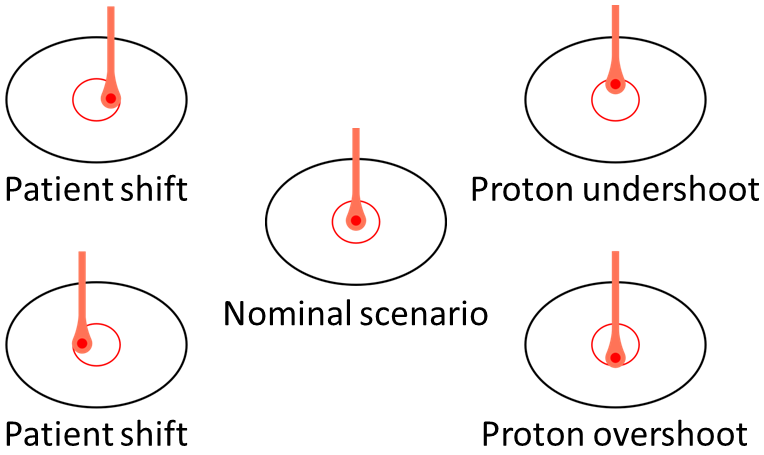

Figure 2.6: Graphical illustration of the error scenarios in robust planning. A beam that deposits its Bragg peak in the center of the target volume (red contour) for the nominal scenario, will deposit this dose in another position when the treatment delivery is subjected to different uncertainties. A robust optimization takes nine error scenarios into account and ensures sufficient target coverage for all these scenarios. Here, the nominal scenario is showed along with two scenarios of patient shift with respect to the beam as well as the two error scenarios for range uncertainties of proton beam, under- and overshoot.

that is robust planning. By definition, a plan is robust when the planned dose and the actual delivered dose are in agreement even in the case of uncertainties [18], and robust planning is hence to optimize the dose delivery in multiple scenarios at once, each scenario taking a different uncertainty into account. There are nine scenarios introduced in an robust optimization and the aim with the robust plan is to fulfill the dose constraints in all scenarios simultaneously, see Figure 2.6 for a schematic illustration. The first scenario to be optimized is the nominal case, which is the undisturbed scenario where everything behaves as it is expected from the planning CT. Next a shift of the patient, with a certain value, is introduced in the $\pm x$-, $\pm y$- , $\pm z$-directions with respect to the beams, respectively. These six different scenarios are meant to account for uncertainties and errors in the patient setup. Lastly there are two cases to simulate range uncertainty, these are over- and undershoot. These features are modelled by two values, one for relative uncertainty and one for absolute uncertainty. Range uncertainties are systematic errors which depend on the CT data on which the treatment plan is made. They can either be the result of CT image artifacts or by patient specific deviations in the conversion between the Hounsfield units, quantifying the grey-scale in the CT image, and the relative proton stopping power [18]. Hence, the quality of the CT will impact the accuracy of the treatment plan. The values for the shifts and for the range are variable and are to be specified in the settings of the treatment planning system.

2.3.2 Interplay effect

The challenge with using a spot scanning technique, such as the IMPT, in treatment of a moving target, like a liver tumor, is that the sensitive spatio-temporal timing of the treatment delivery is compromised. A mismatch in beam deliver with respect to the target position can result in parts of the target being under- or over-dosed. This phenomenon is an example of the so-called interplay effect and this is illustrated in Figure 2.7. In this

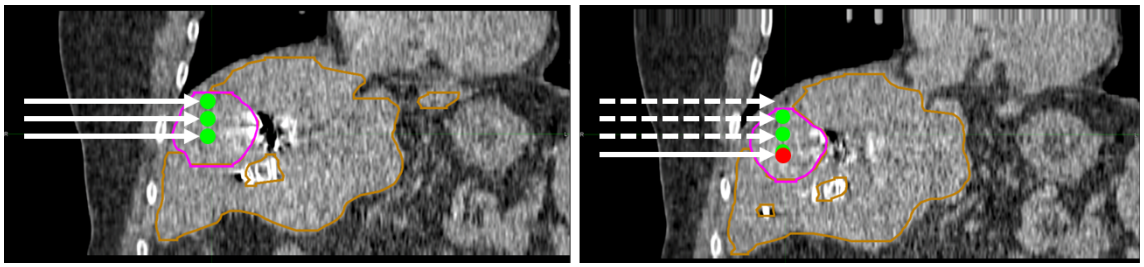

Figure 2.7: Schematic illustration of the interplay effect. The contour in magenta is the CTV and the contour in brown is the healthy liver. To the left, three proton beams deliver dose to the planned position (green circles). When the fourth beam is to be delivered however, the target has moved with respect to the beam and this results in a overlapping of dose spot three and four (red circle). This location in the target will get double dose compared to the planned treatment.

figure, we can see that a movement of the target with respect to the scanning beam results in a specific volume receiving an over-dosage when two (or more) spots overlap, creating a so-called hot-spot. In analogy with this reasoning, over-dosing a part of the volume leads to under-dosing somewhere else when a spot misses its intended position, creating a so-called cold-spot. Such hot- and cold-spots can lead to significant degeneration of the homogeneity of the target dose distribution [19] and how to mitigate this effect will be explained shortly.

Another example of the interplay effect is dose blurring around the edge of the target volume [20]. Contrary to the creation of the hot- and cold-spots in the volume itself, the dose blurring effect can be counteracted by adding a margin around the target [18], such as expanding the target contour to account for all possible positions, or by planning robustly.

2.3.3 Mitigating the interplay effect

There are multiple approaches to mitigate the interplay effect for moving tumors. The idea with these approaches is to either limit the motion of the tumor, controlling the beam or taking the movement into account in the planning. Note that even though measures are taken in trying to mitigate the interplay effect, this effect is still likely to occur because of uncertainties during treatment delivery.

Breath hold

The breath hold approach aims irradiated the target when its motion is restricted [20]. The breath hold "immobilizes" the target and during this time the beam is turned on. A breath hold could either be voluntary or assisted and is usually performed in the end-of-exhalation phase in order to maximize the chance of a good intrafractional reproducibility [4]. An advantage of this technique is that it requires little to no extra equipment on the site of the treatment facility and therefore is easy to implement. A drawback with this approach is that breath holds are not fully reproducible, inevitably leading to an interplay effect in cases when more than one breath hold are needed to complete the treatment.

Beam gating

The idea with gating is similar to the breath hold approach in the sense that the target is only irradiated in one phase, but here the patient is free-breathing during the dose

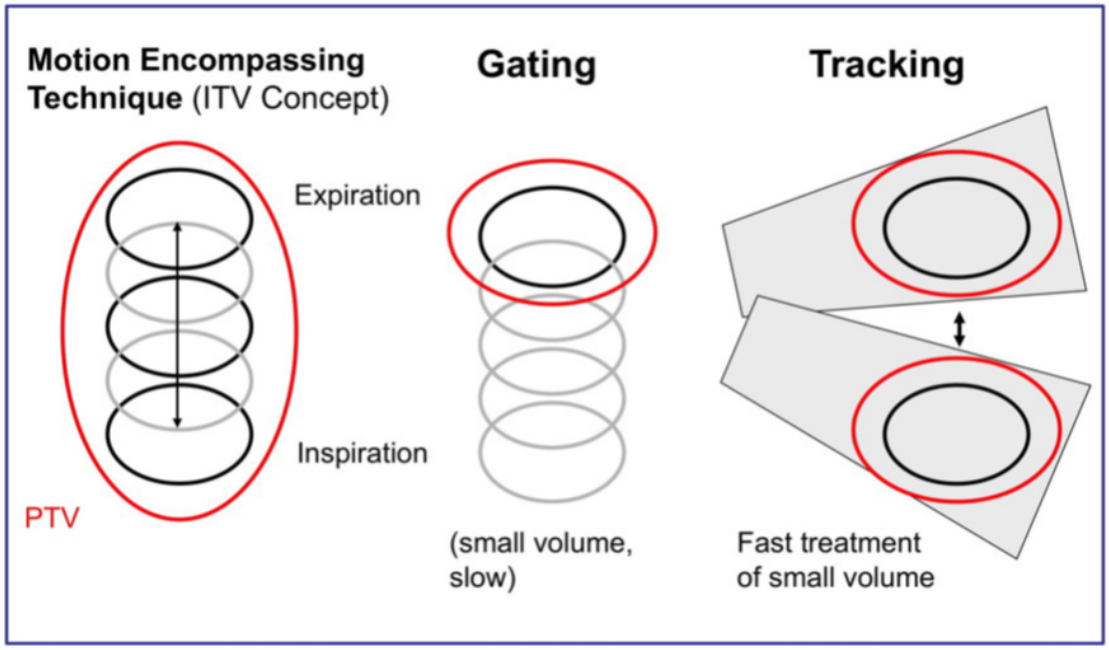

Figure 2.8: Illustration of three different ways of mitigating the interplay effect in radiotherapy. The red contour shows the PTV and can be thought of as the volume that is being irradiated. Left: internal target volume (ITV) approach which encompasses the target in all positions. Middle: beam gating which switches the beam on and off depending on external measurement of breathing. Right: tracking of target motion where the beam follows the target motion. The figure has been adapted from [21].

delivery. The beam is switched on and off during the treatment based on a measurement of a breathing surrogate, such as the motion of the chest wall [20]. This approach is illustrated in the middle of Figure 2.8. The main disadvantage with this approach is that the target can only be irradiated in one phase during free-breathing, and this could lead to prolonged treatment delivery time.

Tumor tracking

The tumor tracking approach is an on-line adaption method which aims to adjust the beam position and energy in real time [20]. This approach requires constant measurements of the tumor position, fiducial markers implanted near the tumor are often used as a surrogate for this. This method is illustrated to the right in Figure 2.8. Tumor tracking is quite complex but has the potential of continuous treatment delivery and thereby shorter the treatment times compared to breath hold or gating.

Rescanning

The idea with rescanning is similar to fractionation; the dose is delivered in smaller parts which sums up to the total dose distribution. The difference being that rescanning is intrafractional, meaning that every dose spot in the volume is irradiated multiple times for each fraction [19]. This approach is meant to average out the interplay effect stemming from overlapping spots since each applied spot now has a lower weight and has the potential of being delivered in a different location with every rescan. This technique has the advantage of being implemented in combination with any of the other interplay mitigating approaches.

There are two different ways of applying rescanning, the first one is called layered rescanning and it scans the each energy layer in the target multiple times before going to the next layer and the second one is called volumetric rescanning and in this approach, the full volume is scanned multiple times. Volumetric rescanning mitigates the interplay effect better than layered rescanning, but it has the drawback of longer irradiation time [19]. In practice, spots with too low weight cannot be delivered because of physical limitations in the treatment delivery system. This restriction introduces a higher limit to how many times rescanning can be applied per fraction.

4D planning

This method tries to account for the tumor movement during the full breathing cycle and is meant for treatment delivery during free-breathing. In this project, 4D planning will be realized either by simultaneously optimizing a treatment plan on multiple breathing phases in a 4DCT or by optimizing a plan on an internal target volume (ITV). An ITV is an expansion of the target volume to cover the CTV in all its possible positions during breathing. The ITV approach is illustrated on the left in Figure 2.8. Delivering a treatment during free-breathing without any tumor tracking has the risk of exposing normal tissue as well as a risk of being subject to interplay, this will be further investigated in this thesis.

2.3.4 Erasmus-iCycle treatment planning system

The treatment planning system (TPS) used in this project is called Erasmus-iCycle [22]. This TPS is a multi-criteria plan, inverse optimizer which has been developed in-house at the Erasmus Medical Center for photon treatment plan generation, and has thereafter been extended for proton therapy planning as well. The optimization is done based on a "wish-list" which specifies prioritization list of dose constraints and objectives for anatomical structures. The dose calculation algorithm is

$$d = Ax, \tag{2.1}$$

where d is the dose distribution vector which holds the dose for each voxel in the patient, A is the dose deposition matrix holding the spacial information of all beamlets, and x is the fluence vector with the weight of each beamlet [22]. The output for the optimization is the fluence vector x.

This TPS always outputs a pareto-optimal plan, which means that none of the optimized constraints or objectives can be improved without worsening another. It uses a random resampling for the placing of the dose spots [23] with a lateral spacing of at least 1 mm. The iterative optimizer was set to stop when no objective could be improved more than 3%. The range of available proton energies is between 70 MeV and 230 MeV and the corresponding spot-sizes for these energies are 7 to 3 mm.

2.4 Treatment evaluation

Treatment evaluation is a validation that the planned treatment actually meets the clinical constraints and hence is clinically acceptable. In order to perform this validation, the three-dimensional dose distribution has to be examined. For the purpose of easier visualization of this quantity in this report however, it is desired to reduce the complexity of the data. The aiding tools for this will be explained in the following sections.

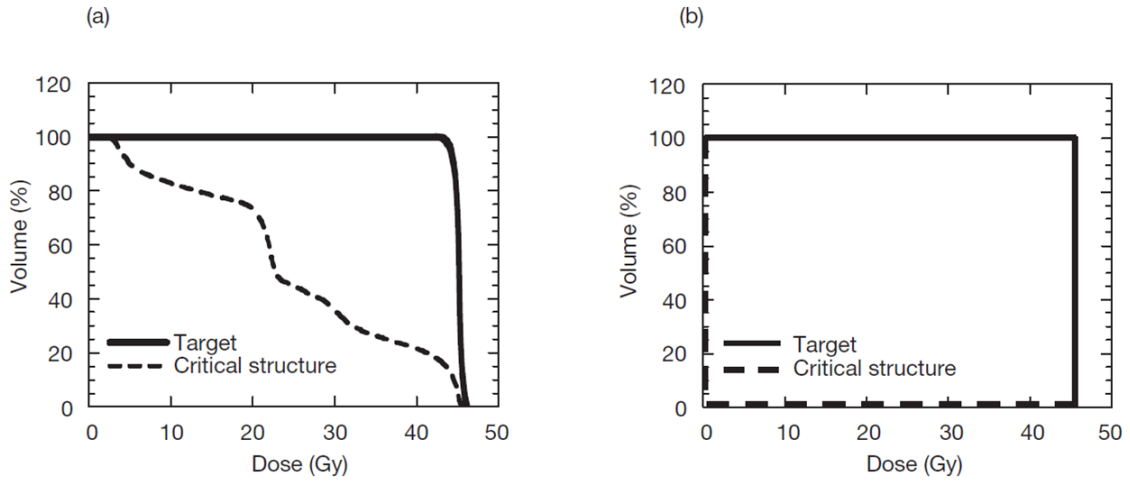

Figure 2.9: (a) Illustration of a clinical DVH where the target is not fully covered by the prescribed dose and the critical structure is exposed. (b) Visualization of an ideal DVH where 100% of the target receives the prescribed dose and the critical structure is fully spared. The figure has been adapted from [9].

2.4.1 Cumulative dose-volume histograms

A cumulative dose-volume histogram (DVH) is a two-dimensional graph showing the dose on the x-axis and percentage of a volume for a structure on the y-axis, and is thereby a simple but still powerful way of visualizing a dose distribution and isodose constraints. Figure 2.9(a) shows an example of a DVH which could be obtained in a clinical setting, with a slight dose fall-off for the target and an exposure of the clinical structure, and Figure 2.9(b) shows an ideal DVH where the full target receives the prescribed dose and the critical structure is completely spared. Note that the resulting DVH for organs which are only partially imaged on a CT scan will be biased since the volume of the imaged organ does not correspond to the percentage on the y-axis [9]. For such cases it would be more informative to choose the y-axis to represent the absolute volume instead of a percentage. Also note that a DVH does not contain any spatial information about the dose and can therefore not be used to compare dose distributions for corresponding voxels [7].

2.4.2 NTCP

A way of describing the dose-volume tolerance for radiation induced liver complications is by means of biological modelling. The normal tissue complication probability (NTCP) is a biological model which aims to describe how well a treatment plan spares the OARs, this based on a single value between 0% and 100%, 0% meaning that the studied organ has no risk of radiation induced complications. Here the NTCP value is obtained for the healthy liver, using the empiric Lyman-Kutcher-Burman model [24]. This model assumes a no threshold sigmoid dose-response relationship according to

$$NTCP = \phi(t) = \frac{1}{\sqrt{2\pi}} \int_{-\infty}^{t} e^{-x^2/2} dx, \tag{2.2}$$

where t is

$$t = \frac{D - TD_{50}(\nu)}{m \cdot TD_{50}(\nu)}. \tag{2.3}$$

D is a value for the deviation of the model parameters and it represents how well the model fits the studied data, the $TD_{50}(\nu)$ is a number that is related with a 50% risk of complications for a uniform irradiation of a part ν of the liver and the parameter m is a characterization of the steepness of the dose response at full organ irradiation ($TD_{50}(1)$). Furthermore, the $TD_{50}(\nu)$ is dependent on the radiation tolerance of the whole liver via the power law relationship

$$TD_{50}(\nu) = TD_{50}(1) \cdot \nu^{-n}. \tag{2.4}$$

In this equation, n is a parameter representing the volume effect of tolerance doses and it relates a uniform irradiation of the whole organ with a uniform irradiation of a part of the organ [24]. When n is near 1, the volume effect is large and when it is near 0, the volume effect is small.

The calculation of the NTCP value for the healthy liver is performed, based on the above described model, in the Erasmus MatterhornRT platform. For this calculation to be possible, the DVH corresponding to a treatment plan first has to be converted to a DVH where the dose delivery is 1.5 Gy per fraction. This conversion is based on the linear-quadratic model using $\alpha/\beta = 2.5$ Gy [25]. The parameter values were chosen as $n = 0.97$, $m = 0.12$ and $TD_{50}(1) = 39.8$ Gy [5, 24, 25].

3

Materials and methods

In this retrospective study, the data from one case of a patient being affected by and treated for hepatocellular carcinoma (HCC) is being used to replan treatments using proton therapy. The treatment modality previously used was stereotactic body radiation treatment (SBRT) utilizing photons and this plan will be used as a baseline in the comparison with and the evaluation of the quality of newly generated proton plans. The simulation of different of different treatment delivery approaches of these proton plans will be explained in this chapter.

3.1 Patient data preprocessing

The three-dimensional planning computed tomography (CT) scan, used for generating and evaluating the photon SBRT plan, can be seen in Figure 3.1. This 3DCT is acquired with the patient in supine position at the end-of-exhalation phase, this is when the lungs are fully deflated and, hence, the diaphragm is in its most superior position.

In order to improve tumor target visibility, the 3DCT scan has been fused with a magnetic resonance imaging (MRI) scan before being contoured by a radiation oncologist. The fusion of the CT and MRI scans is facilitated by four fiducial markers which have been implanted in the liver around the target, these markers can also be used as reference landmarks for the tumor itself. The MRI scan has superior soft tissue contrast in comparison to the CT scan, and this fusion of different image modalities is crucial for an accurate target delineation.

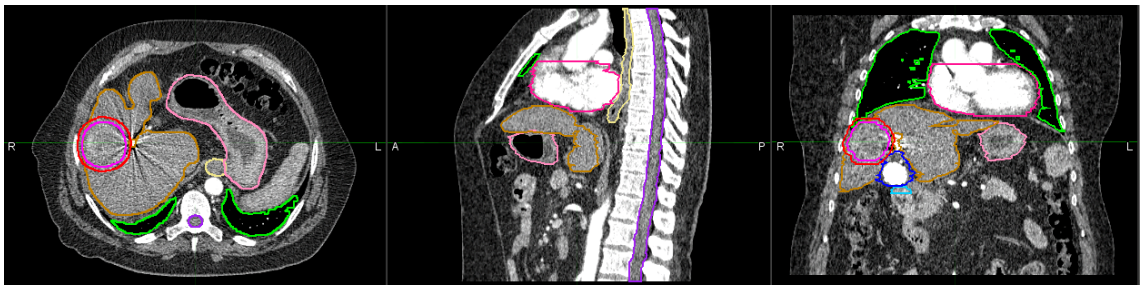

Figure 3.1: Planning CT scan, acquired with fully deflated lungs, which has been used for reference contouring and photon SBRT planning. The left, middle and right image shows the axial, sagittal and coronal plane, respectively. The target CTV (magenta) and PTV (red) can be seen lying inside the liver (brown) which is the main organ at risk. Other organs which are delineated on the planning CT are lungs (green), stomach (pink), heart (deep pink), esophagus (yellow), spinal cord (purple), gallbladder (blue) and duodenum (light blue).

The resolution of the planning CT is $0.92 \times 0.92 \times 1.5$ mm resulting in a grid containing $512 \times 512 \times 224$ voxels. The photon SBRT plan was delivered to the patient using the robotic radiosurgery system CyberKnife 3.5.1 Multiplan 3.5.3 from Accuray Incorporated. This system employs a real-time target tracking system and the dose can therefore be delivered continuously during free-breathing.

3.1.1 4DCT dataset

One four-dimensional computed tomography (4DCT) dataset for the patient has been acquired and this data is used for evaluation of the robustness of static proton plans to perturbations, as well as for the 4D treatment planning. The CT scans were binned to eight different breathing phases for the examined patient, see Figure 3.2. The end-of-exhalation phase is called 0% IN, and it is the phase which is most stable in the breathing cycle in a reproducibility perspective. This phase will be used as the planning phase in the cases for the static proton plans.

The resolution of the 4DCT is $0.71 \times 0.71 \times 2.5$ mm resulting in a grid of $512 \times 512 \times 65$ voxels. This is a slightly better resolution in the axial plane compared to the planning CT, but much worse in the superior-inferior direction. A 4DCT scan inherently takes a longer time to produce than a 3DCT and since there is always a trade-off between CT resolution and scanning time one of the two has to be negotiated given that a prolonged scanning time or an increase of resolution would deliver an additional, unwanted, dose to the patient.

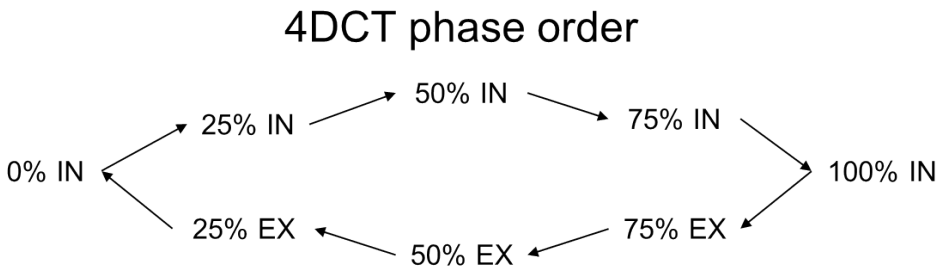

Figure 3.2: Illustration of the order and naming of the eight different 4DCT breathing phases which have been used in this project. The numbers describes the volume of air which the lungs contain in each phase, IN means inhalation and EX means exhalation.

3.1.2 Tumor motion estimation

An estimation of the tumor movement during free-breathing, based on the position of the four fiducial markers in the 4DCT dataset, has been carried out. These fiducial markers are implanted in the liver in the direct proximity of the tumor, meaning that in case of tumor movement there is a corresponding marker movement.

Figure 3.3 shows the position of each marker in the liver. Every CT slice for every phase has been visually examined and the position of each marker, on each phase, has been noted down. Because of the CT image artifacts due to the markers, which are present in the 4DCT datasets, the markers are visible on multiple slices, see Figure 3.3. These image artifacts appear as rays around the markers themselves. For the cases with marker appearance on multiple slices, the intermediate slice with the highest intensity was chosen to represent the position of the marker.

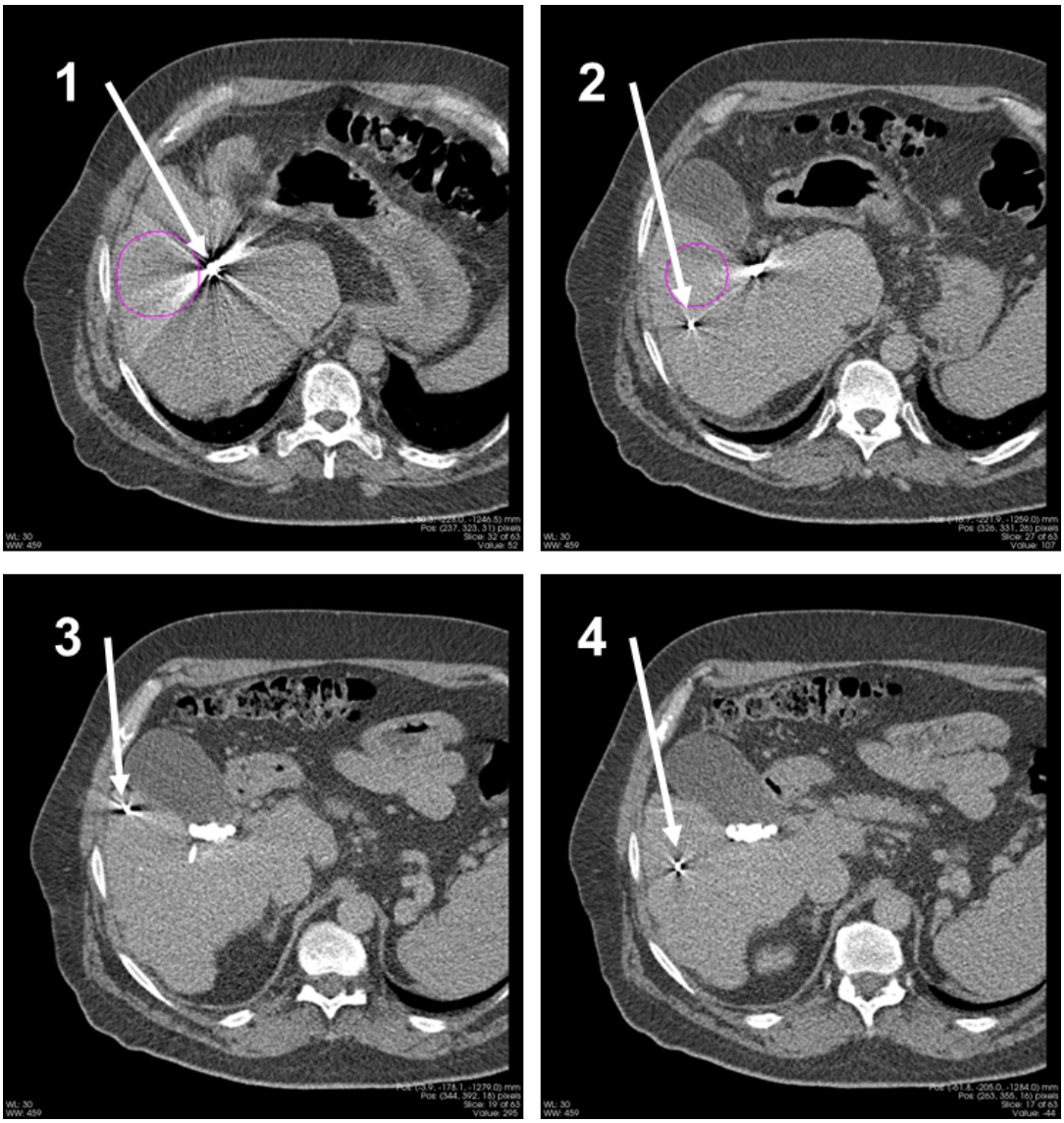

Figure 3.3: Location of the four fiducial markers in the liver indicated by the arrows. Marker 1 is the most superior (uppermost) marker, and Marker 4 is the most inferior (lowermost) marker. The CTV contour can be seen in magenta in the two upper images.

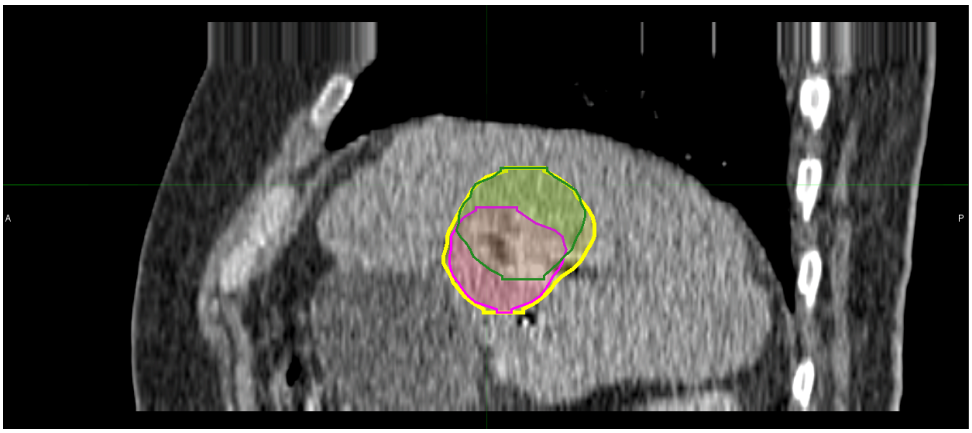

Figure 3.4: Extension of the ITV (yellow) on a slice on the sagittal plane from the 50% EX 4DCT. The ITV contour encompasses the CTV in all phases. The most extreme positions of the CTV are also visualized; 0% IN in superior position (green) and 100% IN in inferior position (magenta).

3.1.3 4DCT contouring

The contouring of all structures were done using MIM Maestro (MIM Software Inc.). The original delineations, made by a radiation oncologist on the 0% IN planning CT, have been used as a basis when contouring the full 4DCT dataset. The structures which were included in this set were; CTV, PTV, duodenum, esophagus, gallbladder, heart, right kidney, liver, liver-CTV ("liver minus CTV", referring to the healthy liver), left lung, right lung, spinal cord, stomach and a patient contour separating the body from the surroundings. No margin has been applied between the GTV and the CTV. The left kidney did not appear on the CT image due to its inferior position, and was therefore not delineated. All these contours were copied from the 0% IN planning CT to the 0% IN phase in the 4DCT and corrected slightly in order to fit the current anatomy. After this, the contours on the 0% IN phase in the 4DCT were propagated on to all other phases using a built-in MIM-function called "Sequential Deformable Propagation". This function uses an algorithm which is CT image intensity-based, and hence tries to make sure that each contour has the same "grey-scale" inside the propagated contour on the new CT as for the reference contour on the old CT. Since the grey-scale in a CT is proportional to the density of a tissue, this means that the algorithm works best in the case when all contours hold tissues or organs with clearly separable densities as it would lead to greater contrast in the CT values. As the name of the algorithm suggests, it propagates the contours in a sequential manner meaning that the it first propagates the contours from 0% IN to 25% IN, then from 25% IN to 50% IN, and so forth until the starting phase is reached.

Because the resolution of the 4DCT dataset is quite low and because of poor soft tissue contrast of CT itself, the resulting contour sets from the propagation algorithm had to be reviewed and corrected on all slices and for every phase. The CTV and PTV contours were also reviewed and corrected based on the movement of the surrounding markers. The tumor is not visible on the CT itself, and the markers are hence needed as landmarks to be able to contour this structure realistically during motion due to the breathing. As an extra help in the CTV and PTV contour correction step, it was assumed that the volume of these structures would not change significantly during the breathing cycle, hence no deformation of the target, and they were therefore kept to be approximately 80 cm^3 and 140 cm^3, respectively.

In order to be able to make a 4D proton plan, an internal target volume (ITV) for the CTV was also created. The ITV encompasses the all possible positions of the CTV during the breathing motion, see illustration on the sagittal plane in Figure 3.4. The volume of the ITV for the CTV was 120 cm^3 and it was contoured on the phase of 50% EX in the 4DCT.

3.2 Treatment plan generation

The IMPT treatment plans were optimized using Erasmus-iCycle. The inputs to this optimizer are a delineated CT scan, representing the anatomy of the patient, and a list with prescription doses to the organs and structures visible on the CT scan. The list with dose prescriptions is called a "wish-list" and such a list does not only hold the information about the dose constrains, but also about which order the doses should be optimized, the chosen beam angles, the robustness settings, which method the optimizer should use to reach the final plan and the criterion for when to stop optimizing.

The basis for the proton wish-lists, to be presented, is a photon wish-list for the treatment of liver HCC. That wish-list has gradually been adjusted to fit the case for IMPT better. Making a wish-list is an iterative procedure to allow for tweaking of a new version by incorporating knowledge from earlier simulations. The "Priority" column in a wish-list specifies in which order the doses are to be optimized and whether they are constraints or objectives (decreasing importance with higher number) and the "Type" column defines how these doses should be optimized. "Linear" optimization means that all voxels, of a specific structure taken into account in the optimization, should meet the assigned dose constraint and "Mean" optimization implies that the mean dose of all voxels, which are optimized, should meet the assigned minimum or maximum dose. Both "Linear" and "Mean" optimization can be applied to the same structure in a wish-list.

3.2.1 Dose prescriptions and constraints

The photon SBRT dose prescription for the examined patient was 6×8 Gy at 80% isodose to the PTV, resulting in a dose of 48 Gy to this structure. This means that the treatment is delivered in six fractions, each with the goal of delivering 8 Gy to the PTV. Prescribing at 80% isodose level implies that 100% dose is the maximally allowed dose, D_{max}, in the volume. For this case, the maximum dose is $D_{max} = \frac{48\,\text{Gy}}{0.80} = 60\,\text{Gy}$. Prescribing the dose in this manner also implies that 90% isodose preferably should encompass the whole CTV. Because of limitations in plan optimization, however, the clinically acceptable constraint is that 90% isodose is encompassing 95% of the CTV. For a full list of constraints on the target and the organs at risks (OARs), see Table 3.1.

The dose prescriptions for the IMPT treatment plans were made to mimic the photon SBRT plan's CTV coverage at the same time as trying to minimize the dose to the OARs. Therefore, the dose prescription to the CTV will always be prescribed as maximizing the minimum dose to 54 Gy (90% isodose) while minimizing the maximum to $D_{max} = 60$ Gy. The only exception to this is when dose escalation is applied, and the maximally allowed dose, D_{max}, can then be increased.

In order to further mimic the photon SBRT plans with the IMPT therapy plans, it is desired to push the dose up towards the maximally allowed dose, D_{max}, in the middle of the target. This is done by creating structures within the CTV itself and prescribe a higher dose to them. The higher dose for the new structures should be in the range of the 90% isodose prescribed to the CTV and the maximally allowed dose, D_{max}.

Table 3.1: Constraints and objectives on target volumes and organs at risk for photon SBRT treatment plans utilizing photons. This protocol for dose prescription is clinically used at Erasmus Medical Center [25].

Organ or structure	Hard constraints
PTV	$D_{max} < 60\,\text{Gy}$
	48 Gy = 80% isodose should encompass > 95% of the PTV
CTV	54 Gy = 90% isodose should encompass > 95% of the CTV
	D_{mean} to liver-CTV $< 22\,\text{Gy}$
Healthy liver	NTCP for liver-CTV$\leq 5\%$
	$> 800\,\text{cm}^3$ of liver-CTV receives a dose $< 23.4\,\text{Gy}$
Stomach	$D_{max} < 39\,\text{Gy}$ and volume receiving $\geq 30\,\text{Gy}$ should be $\leq 5\,\text{cm}^3$
Duodenum	$D_{max} < 39\,\text{Gy}$
Esophagus	$D_{max} < 36\,\text{Gy}$
Spinal cord	$D_{max} < 24\,\text{Gy}$
Kidney	2/3 of the right kidney $< 19.2\,\text{Gy}$
	Objectives
Heart	$D_{max} < 39\,\text{Gy}$
Gallbladder	$D_{max} < 60\,\text{Gy}$
Skin	D_{max} to a volume of $0.5\,\text{cm}^3 < 34.8\,\text{Gy}$

3.2.2 3D non-robust plan with dose escalation

The wish-list used for making the 3D non-robust IMPT plans, to be delivered when the patient holds his or her breath, can be found in Table 3.2. The optimization done with this wish-list was planned on the breathing phase of 0% IN with isocenter of the beams in the CTV. Three different levels of dose escalation were investigated for this approach. Dose escalation means that a higher maximum dose to the target is allowed, and it is implemented in the wish-list by multiplying a dose escalation factor with the goal dose of 60 Gy (on the second line in Table 3.2). The investigated levels of dose escalation were 105%, 120% and 140%. All further analysis of the 3D non-robust plans are made with the plan with 140% dose escalation, the reason for that being that it is the plan which should spare the surrounding tissues best because it allows for high in-field dose gradients. This wish-list uses three co-planar beams with a beam configuration of 0°, −70° and −120°.

3.2.3 3D robust plan

The wish-list used for making the 3D robust IMPT plan can be found in Table 3.3. This plan is to be delivered to the patient during breath hold. The optimization done with this wish-list was planned on the breathing phase of 0% IN with isocenter of the beams in the CTV. The robustness settings used for this were 5 mm setup robustness and 3.5% relative value and 1 mm absolute value for the range robustness. For this case, dose in the rings surrounding the CTV could be prescribed to a lower dose than in the case of the 3D non-robust wish-list. This does not mean that the optimizer was able to meet these values, but that it was encouraged to try to decrease the dose in these areas. This way of prescribing the dose did not compromise the CTV coverage in the optimized plan. This wish-list uses three co-planar beams with a beam configuration of 0°, −70° and −120°.

Table 3.2: Non-robust wish-list used for 3D optimization. In case of dose escalation, the dose goal on the first line would be increased by a multiplication factor of either 1.05, 1.20 or 1.40.

Priority	Structure	Min/Max	Type	Goal	Robust
1	CTV	Minimize maximum	Linear	60 Gy	No
Constraint	CTV	Maximize minimum	Linear	0.90×60 Gy	No
Constraint	CTV higherdose	Maximize minimum	Linear	0.98×60 Gy	No
Constraint	CTV highdose	Maximize minimum	Linear	0.95×60 Gy	No
1	CTV ring 0-5	Minimize maximum	Linear	0.90×60 Gy	No
2	CTV ring 5-10	Minimize maximum	Linear	0.85×60 Gy	No
2	CTV ring 10-15	Minimize maximum	Linear	0.75×60 Gy	No
3	CTV ring 15-25	Minimize maximum	Linear	0.50×60 Gy	No
3	External ring	Minimize maximum	Linear	0.15×60 Gy	No
4	Liver-CTV	Minimize maximum	Mean	1 Gy	No
4	Liver-CTV	Minimize maximum	Linear	1 Gy	No
5	Stomach	Minimize maximum	Linear	1 Gy	No
5	Duodenum	Minimize maximum	Linear	1 Gy	No
6	Esophagus	Minimize maximum	Linear	1 Gy	No
6	Spinal cord	Minimize maximum	Linear	1 Gy	No
7	Right kidney	Minimize maximum	Mean	1 Gy	No
7	Heart	Minimize maximum	Linear	1 Gy	No
8	Gallbladder	Minimize maximum	Linear	1 Gy	No
9	Monitor units (Giga protons)	Minimize maximum	Linear	1	No

Table 3.3: Robust wish-list used for 3D optimization. Robustness settings: 5 mm for setup errors and 3.5% relative and 1 mm absolute for range errors.

Priority	Structure	Min/Max	Type	Goal	Robust
Constraint	CTV	Minimize maximum	Linear	60 Gy	Yes
Constraint	CTV higherdose	Maximize minimum	Linear	0.98×60 Gy	Yes
Constraint	CTV highdose	Maximize minimum	Linear	0.95×60 Gy	Yes
1	CTV	Maximize minimum	Linear	0.90×60 Gy	Yes
1	CTV ring 0-5	Minimize maximum	Linear	0.70×60 Gy	Yes
2	CTV ring 5-10	Minimize maximum	Linear	0.50×60 Gy	Yes
2	CTV ring 10-15	Minimize maximum	Linear	0.30×60 Gy	Yes
3	CTV ring 15-25	Minimize maximum	Linear	0.15×60 Gy	Yes
3	External ring	Minimize maximum	Linear	0.10×60 Gy	Yes
4	Liver-CTV	Minimize maximum	Mean	1 Gy	Yes
4	Liver-CTV	Minimize maximum	Linear	1 Gy	Yes
5	Stomach	Minimize maximum	Linear	1 Gy	Yes
5	Duodenum	Minimize maximum	Linear	1 Gy	Yes
6	Esophagus	Minimize maximum	Linear	1 Gy	Yes
6	Spinal cord	Minimize maximum	Linear	1 Gy	Yes
7	Right kidney	Minimize maximum	Mean	1 Gy	Yes
7	Heart	Minimize maximum	Linear	1 Gy	Yes
8	Gallbladder	Minimize maximum	Linear	1 Gy	Yes
9	Monitor units (Giga protons)	Minimize maximum	Linear	1	Yes

3.2.4 4D non-robust plan for optimization on multiple CTs

The wish-list used for optimizing a 4D non-robust plan on multiple phases at once can be found in Table 3.4. The aim of this 4D plan is to fulfill the dose constraints on all breathing phases simultaneously and the patient is meant to be irradiated continuously during free-breathing. The optimization done with this wish-list was planned on the phases 0% IN, 50% EX and 100% IN with the CTV on 50% EX as isocenter for the beams. In order not to introduce interfering constraints when optimizing on multiple phases at the same time the CTV rings, where the dose is usually being pushed down, have been removed from this wish-list. If the rings would still have been in the wish-list, these structures would have overlapped with the target volume when going from one phase to the other. The wish-list uses three co-planar beams with a beam configuration of $0°$, $-70°$ and $-120°$.

Table 3.4: Non-robust wish-list used for optimizing a 4D plan on multiple CTs at once. Notice that the CTV rings have been removed from this wish-list.

Priority	Structure	Min/Max	Type	Goal	Robust
Constraint	CTV	Minimize maximum	Linear	60 Gy	No
Constraint	CTV higherdose	Maximize minimum	Linear	0.98×60 Gy	No
Constraint	CTV highdose	Maximize minimum	Linear	0.95×60 Gy	No
1	CTV	Maximize minimum	Linear	0.90×60 Gy	No
3	External ring	Minimize maximum	Linear	0.10×60 Gy	No
4	Liver-CTV	Minimize maximum	Mean	1 Gy	No
4	Liver-CTV	Minimize maximum	Linear	1 Gy	No
5	Stomach	Minimize maximum	Linear	1 Gy	No
5	Duodenum	Minimize maximum	Linear	1 Gy	No
6	Esophagus	Minimize maximum	Linear	1 Gy	No
6	Spinal cord	Minimize maximum	Linear	1 Gy	No
7	Right kidney	Minimize maximum	Mean	1 Gy	No
7	Heart	Minimize maximum	Linear	1 Gy	No
8	Gallbladder	Minimize maximum	Linear	1 Gy	No
9	Monitor units (Giga protons)	Minimize maximum	Linear	1	No

3.2.5 4D robust plan ITV

The wish-list used for optimizing a 4D robust ITV plan can be found in Table 3.5. As mentioned before, the ITV encompasses all possible CTV positions during free-breathing, and the goal with this plan is hence to have sufficient dose coverage of the CTV on all breathing phases as this plan is to be delivered continuously during free-breathing. The optimization done with this wish-list was planned on the phase of 50% EX, because this phase is assumed to have the most average anatomy, with the isocenter of the beams in the ITV. This wish-list is actually the same wish-list as for the 3D robust plan, only replacing the CTV with the ITV, and it uses the same robustness settings of 5 mm setup robustness and 3.5% relative value and 1 mm absolute value for the range robustness. This plan uses three co-planar beams with a beam configuration of $0°$, $-70°$ and $-120°$.

3.3 Simulation of treatment delivery

All treatment plans are made on a set of rigid CT images. When these plans are delivered, however, the anatomy will never be identical to the planning scenario and simulations of these non-ideal scenarios are needed in order for a fair evaluation of the treatment prospects

Table 3.5: Robust wish-list used for the 4D ITV optimization. Robustness settings: 5 mm for setup errors and 3.5% relative and 1 mm absolute for range errors.

Priority	Structure	Min/Max	Type	Goal	Robust
Constraint	ITV	Minimize maximum	Linear	60 Gy	Yes
Constraint	ITV higherdose	Maximize minimum	Linear	0.98×60 Gy	Yes
Constraint	ITV highdose	Maximize minimum	Linear	0.95×60 Gy	Yes
1	ITV	Maximize minimum	Linear	0.90×60 Gy	Yes
1	ITV ring 0-5	Minimize maximum	Linear	0.70×60 Gy	Yes
2	ITV ring 5-10	Minimize maximum	Linear	0.50×60 Gy	Yes
2	ITV ring 10-15	Minimize maximum	Linear	0.30×60 Gy	Yes
3	ITV ring 15-25	Minimize maximum	Linear	0.15×60 Gy	Yes
3	External ring	Minimize maximum	Linear	0.10×60 Gy	Yes
4	Liver-CTV	Minimize maximum	Mean	1 Gy	Yes
4	Liver-CTV	Minimize maximum	Linear	1 Gy	Yes
5	Stomach	Minimize maximum	Linear	1 Gy	Yes
5	Duodenum	Minimize maximum	Linear	1 Gy	Yes
6	Esophagus	Minimize maximum	Linear	1 Gy	Yes
6	Spinal cord	Minimize maximum	Linear	1 Gy	Yes
7	Right kidney	Minimize maximum	Mean	1 Gy	Yes
7	Heart	Minimize maximum	Linear	1 Gy	Yes
8	Gallbladder	Minimize maximum	Linear	1 Gy	Yes
9	Monitor units (Giga protons)	Minimize maximum	Linear	1	Yes

of IMPT for HCC. All plans, both in the simulation and in actual future applications, deliver the dose to the patient spot per spot, switching the beam on and off until the whole target is scanned. The beam-on-time, the beam movement time, the energy layer switching time and the beam switching time have all been taken into account in the simulations of the treatment delivery. The treatment delivery, both for the 3D and the 4D plans, is simulated to be delivered in one fraction, six fraction and six fractions with three times volumetric rescanning, respectively. All modelling and simulation has been carried out using MATLAB (MathWorks).

3.3.1 Breath hold interplay

The idea of this simulation is to test the treatment delivery of the 3D plans in a breath hold scenario to be able to evaluate the impact of the interplay due to imperfect breath hold reproducibility. The 3D treatments are planned on the 0% IN phase and the aim is to deliver the dose in this end-of-exhalation breath hold. In reality, however, breath holds are not fully reproducible, meaning that every new breath hold is unique and slightly changes the anatomy of the target giving rise to the interplay effect. This characteristic of non-reproducible breath holds is modelled by randomly giving one breath hold worth of spots not only to the 0% IN phase, but also to the adjacent 25% EX and 25% IN phases. Figure 3.5 shows the same CT slice from the three different phases included in the analysis. The slight change of anatomy, illustrated in this figure, will perturbate the dose distribution and also introduce the risk of missing the target. In this study, one breath hold is set to be 20 sec. The selection of which CT the dose is delivered to in every breath hold is determined by a uniform random distribution.

After the full treatment has been delivered, spot by spot to one randomly chosen phase in every new breath hold, the spots have to be summed to form a final dose distribution. This dose distribution is to be evaluated on the 0% IN reference phase, so in order to get the contribution from the spots delivered to the phases of 25% EX and 25% IN these have

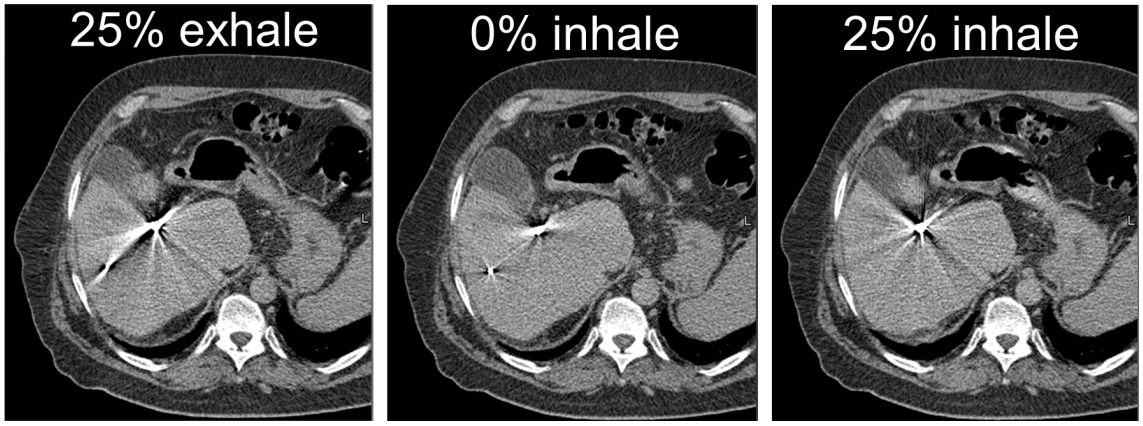

Figure 3.5: CT images with slices in the axial plane from the same SI position, for different phases in the 4DCT. Notice that the anatomy is unique on each phase.

to be transformed to the reference phase. The transformations were done in the Erasmus MatterhornRT platform, using the method of non-rigid B-spine vector field based on the grey value of the CT image. The final distribution is then obtained by addition of the (transformed) dose matrices for every spot.

The breath hold interplay simulation, described above, has been run for both the 3D non-robust plan and the 3D robust plan. The nominal case and all error scenarios have been analyzed separately with a sample size of 100 for each fractionation scheme. For the case with the non-robust plan, this means that the dose first had to be distorted to get the information about the error scenarios. The values used for the distortion were the same as used in the planning of the robust plan (5 mm for setup and 3.5% relative and 1 mm absolute for range).

In addition to the study of every error scenario separately, a sensitivity analysis has also been carried out for the breath hold interplay. This sensitivity analysis, as well as the regular breath hold interplay simulation, simulates irradiation in breath hold but with the difference that now every fraction is being perturbed by a different error scenario and is, hence, a simulation of a more realistic treatment than studying every scenario separately. The scenarios taken into account here were the nominal case and positive or negative shifts in x-, y- and z-direction. Overshoot and undershoot are excluded since they are systematic errors and in reality would influence a whole treatment and not just a single fraction. The choice of error scenario for each new fraction was randomly drawn from a uniform distribution. The sample size for this analysis was 1000 samples for every fractionation scheme for both the 3D non-robust and the 3D robust plan.

3.3.2 4D interplay

The simulation of the 4D interplay simulates the delivery of a treatment during free-breathing and it tests the 4D plans. The treatment is delivered spot by spot to one of the phases in the 4DCT and the contribution from each phase is then transformed to the 0% IN reference phase in order for summation to get the final dose distribution, this with the same analogy as for the breath hold interplay.

A breathing signal, sampled from a real case scenario of photon therapy delivery with CyberKnife, is used for determining a probability distribution for the length of breathing periods. Ideal breathing signals of different periods, τ, matching the probability distribu-

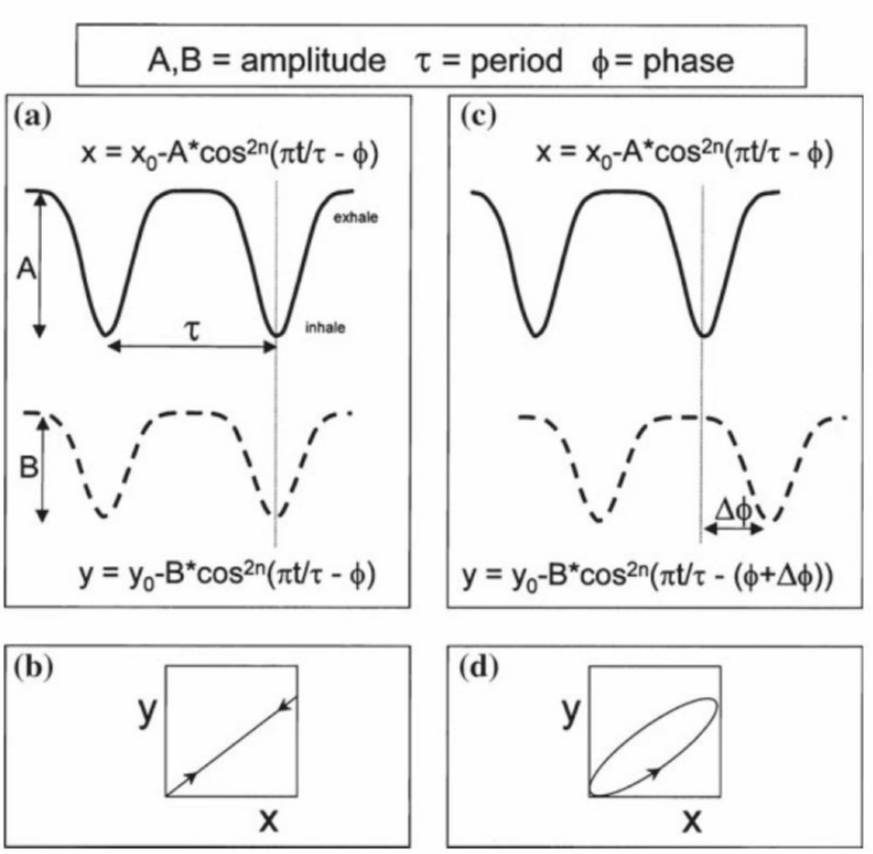

Figure 3.6: Ideal modeling of breathing pattern with cosines in two directions perpendicular to each other. (a) and (b) illustrates the motion when the two directions are in phase and (c) and (d) illustrates when they are out of phase, this is called hysteresis. The figure has been adapted from [26].

tion obtained from the sampled signal are then consecutively place behind each other to model the breathing signal (for free-breathing) for the entire treatment. This breathing signal is used in the simulation of the dose delivery and it decides which phase, in the 4DCT, a specific spot is delivered to.

An ideal breathing period is modelled as shown in Figure 3.6. In (a) and (b) in this figure it is assumed that motion in different directions, for example superior-inferior for x and anterior-posterior for y, are in phase. This leads to the tumor motion being modelled in a linear way. In (c) and (d) it is assumed that the motion in different directions are out of phase, leading to hysteresis. Hysteresis basically means that the motion of the tumor can be different for inhalation and expiration, implying that the tumor position would be different on 50% IN compared to 50% EX. This model of the hysteresis is not taken into account for this interplay analysis with the 4D plan however, and therefore only (a) and (b) are applicable for this study, leading to the use of five out of eight phases from the 4DCT scan in this simulation. The phases used were 100% IN, 75% EX, 50% EX, 25% EX, and 0% IN, all from exhalation.

The above described 4D interplay analysis has been run for the 4D robust ITV plan. In analogy with the breath hold interplay, the nominal case and all the error scenarios have been analyzed separately with a sample size of 100 simulated treatments for every fractionation scheme. No sensitivity analysis has been carried out for this simulation.

3.4 Evaluation of treatment plans

The treatment plans have to be evaluated in order to see if they meet the clinical constraints or not. They also need to be compared with the photon SBRT plan in order to draw conclusions about advantages and drawbacks of using IMPT for HCC. All plans have been evaluated statically and three of the four plans have also been evaluated by means of simulating treatments.

3.4.1 Static evaluation

The dose distributions for all plans have to be evaluated and compared to the photon SBRT plan. The 3D plans have been evaluated on the phase of 0% IN, on which they were planned, but also on the phases of 25% IN and 25% EX. The last evaluation is to serve as a verification of the breath hold interplay. The 4D plans have also to be statically evaluated on the phase of 50% EX, on which they were planned, but also on all other phases in the 4DCT. This is because tumor coverage in all possible positions is essential for a successful treatment delivery during free-breathing.

All static evaluations of the target coverage and the dose to the OARs is to presented using cumulative dose-volume histograms (DVHs), in such a graph one can easily examine all the dose constraint stated in Tabel 3.1. For further evaluation of the proton plans, the value of the normal tissue complication probability (NTPC) for the liver-CTV will be stated and compared with the photon plan.

3.4.2 Simulation of treatment – Interplay analyses

For the interplay simulations, where treatment delivery has been simulated multiple times for every fractionation scheme and every treatment plan, the statistics from these results will be shown. Focus will here lie on examining the 90% isodose coverage to the CTV as well as the volume of the CTV getting more than the prescribed dose, indicating that there are hot-spots (over-dosage) in the volume. Also the dose to the liver-CTV will be evaluated since it is the main OAR in this study.

The data will be presented in boxplots, comparing different fractionation schemes as well as different error scenarios and different treatment plans. DVH curves showing low dose scenario, high dose scenario, average dose scenario and the optimized scenario will also be presented. It should be noted here that the low and the high dose scenarios are not the most extreme simulated samples separately, but the minimum and the maximum dose scenario for all the simulated treatments analyzed together.

4

Results

In this chapter, all the relevant results from this study will be presented. The treatment evaluation will first be done separately for every plan and simulation approach and they will then be compared among each other. Each error scenario will be studied separately in order to draw conclusions of their impact on the treatment, see Table 4.1 for an overview and a short description of the error scenarios at hand. The main focus in this chapter will be to examine the dose coverage of the clinical target volume (CTV) and the dose to the main organ at risk (OAR), which is the healthy liver, as well as to compare the photon and the proton plans. For some cases, also the dose to the gallbladder and the heart will be shown in dose-volume histograms (DVHs).

Table 4.1: The plans are evaluated for a total of nine different error scenarios, described below. The x-axis lies in the left-right (LR) direction, the y-axis in the anterior-posterior direction and the z-axis in the superior-inferior direction. The shifts tests the setup robustness of 5 mm and over- and undershoot scenarios are the worst case range scenarios based on 3.5% relative value and 1 mm absolute value.

Error scenario	Description
Error 1	Nominal (undisturbed) scenario
Error 2	Shift in $+x$-direction
Error 3	Shift in $+y$-direction
Error 4	Shift in $+z$-direction
Error 5	Shift in $-x$-direction
Error 6	Shift in $-y$-direction
Error 7	Shift in $-z$-direction
Error 8	Overshoot
Error 9	Undershoot

An illustration of the plots which will be shown in this chapter can be found in Figure 4.1. A DVH curve showing CTV coverage is shown on the left in this figure, such an illustration is meant to show what percentage of the volume of a structure or organ receives a specific dose. The black dotted lines in this plot visualize the clinical dose-volume constraint for the CTV of 90% isodose encompassing 95% of the volume. Since this constraint is a restriction on the minimum dose to the CTV, the dose plan meets this constraint if the DVH curve passes on the upper-right side of the cross-section between these two dotted lines. When the clinical constraint for the liver-CTV will be shown later on, the dose plans meet the clinical dose-volume constraint if they pass the cross-section on the lower-left side, this because it is a restriction on the maximum dose to the structure. To the right in the same figure, a boxplot showing statistics for the volume of the CTV receiving $\geq 90\%$ of the prescribed dose is shown, illustrating the result from one of the interplay simulations. The red line in this plot shows the median of the data, the edges

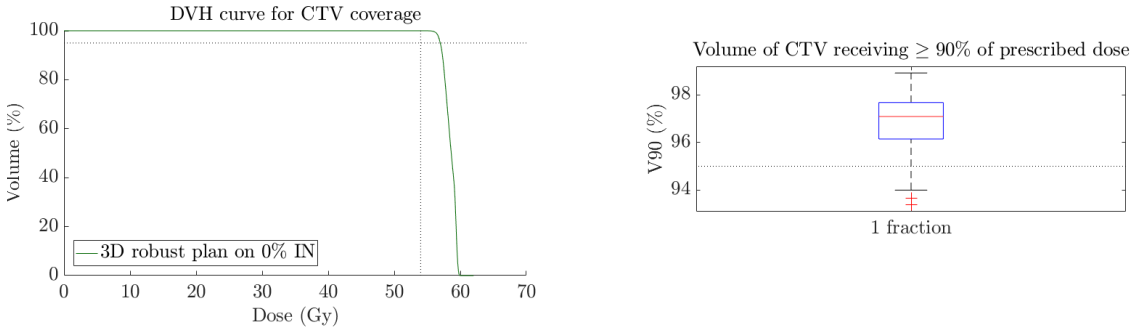

Figure 4.1: Illustration of the plots which are to be presented in this chapter. An example of a DVH curve is visualized on the left and an example of a boxplot is visualized on the right.

of the box shows the 25$^{\text{th}}$ and 75$^{\text{th}}$ percentiles, the whiskers show the most extreme data points and the individual marks are considered to be outliers. The black dotted line is, again, illustrating the clinical dose-volume constraint for the CTV. This constraint is met for all samples in the simulation if all data is plotted above this dotted line. Ideally, the volume of the CTV receiving 90% of the prescribed dose should be 100% for every simulated treatment, meaning that the box would be compressed on the red (median) line and that this line would be located on the level of the 100% marking on the y-axis. For comparison of the CTV coverage between the proton plan and the photon SBRT plan, a red dotted line will be plotted in the boxplots. If the simulation of the IMPT plan delivery performs better than the ideal photon SBRT treatment, the boxes will be plotted above this red dotted line. When it is the volume of the CTV receiving $\geq 100\%$ of the prescribed dose will be studied (instead of the volume receiving $\geq 90\%$ of the prescribed dose) this value is ideally as low as possible, indicating that there are few hot-spots in the volume.

4.1 Tumor motion estimation

After the estimation of the tumor movement, based on the movement of the fiducial markers, it can be established that the most prominent direction of the movement is the superior-inferior (SI) direction, followed by the anterior-posterior (AP) direction and lastly the left-right (LR) direction, see Table 4.2. This is consistent with measurement and estimations which can be found in literature [27].

The largest difference in position can be found for Marker 3 between the 0% IN and 100% IN phases, where the absolute difference between the extreme values in the SI direction is 17.5 mm. The total motion of Marker 3, calculated with the Euclidean norm by taking the movement in AP and LR direction into account, is about 20 mm. It should be noted here that errors in the motion estimation depends on computed tomography (CT) image artifacts as well as on human error in the visual examination of the images. Since the CT resolution is coarsest in the SI direction (2.5 mm between two consecutive slices), the error is assumed to be largest in this direction with ± 2.5 mm. In the AP and LR directions, the CT grid is much finer and the error should not be greater than ± 1 mm.

Based on Table 4.2, we can see that the difference in the marker position between two corresponding phases in inhalation and in exhalation is smaller than 3 mm in all directions. Even though this difference in position is not very large for the examined patient, it still indicates that the result from a simulation of the interplay would be more realistic if hysteresis was to be taken into account.

Table 4.2: Marker position for all four markers on each breathing phase. The x-axis lies in the left-right (LR) direction, the y-axis in the anterior-posterior direction and the z-axis in the superior-inferior direction. All coordinates are given in millimeters.

	Marker 1 (uppermost)			Marker 2			Marker 3			Marker 4 (lowermost)		
Phase	x (LR)	y (AP)	z (SI)	x (LR)	y (AP)	z (SI)	x (LR)	y (AP)	z (SI)	x (LR)	y (AP)	z (SI)
0% IN	-77.9	-265.8	-1249	-116.3	-229.4	-1259	-133.6	-284.8	-1279	-124.7	-247.4	-1284
25% IN	-77.7	-268.3	-1251.5	-117	-232	-1264	-133.1	-288.5	-1286.5	-126	-250.7	-1289
50% IN	-79.5	-270.3	-1254	-118.9	-233.7	-1266.5	-133.8	-291.6	-1291.5	-126.6	-253.6	-1294
75% IN	-79.9	-271.7	-1256.5	-119.3	-236.4	-1271.5	-133.8	-293	-1294	-127	-255.4	-1296.5
100% IN	-79.9	-274	-1259	-120.5	-236.9	-1274	-134.1	-294.3	-1296.5	-127.3	-256.4	-1299
75% EX	-79	-271.3	-1256.5	-119.6	-235.6	-1269	-134.1	-292	-1291.5	-126.8	-254.1	-1294
50% EX	-76.6	-269.2	-1254	-117	-233.1	-1264	-133.4	-291	-1289	-126.2	-253	-1291.5
25% EX	-76.6	-268.6	-1251.5	-116.2	-231.4	-1261.5	-133.5	-287.3	-1284	-125.1	-249.6	-1289
Absolute max-min difference	3.3	8.2	10	4.3	7.5	15	1	9.5	17.5	2.6	9	15

4.2 3D non-robust plan with dose escalation

A static evaluation of the DVHs for the 3D non-robust plans with different levels of dose escalation, in comparison with the SBRT photon plan, can be found in Figure 4.2. These dose distributions are evaluated on the 0% phase, on which they are planned, for the CTV, the liver-CTV, the gallbladder and the heart. From this figure we can see that the non-robust proton plans have better CTV coverage than the photon plan and that they at the same time they have better sparing of the OARs. The clinical constraints, from Table 3.1, are all met for the proton plans in this stage.

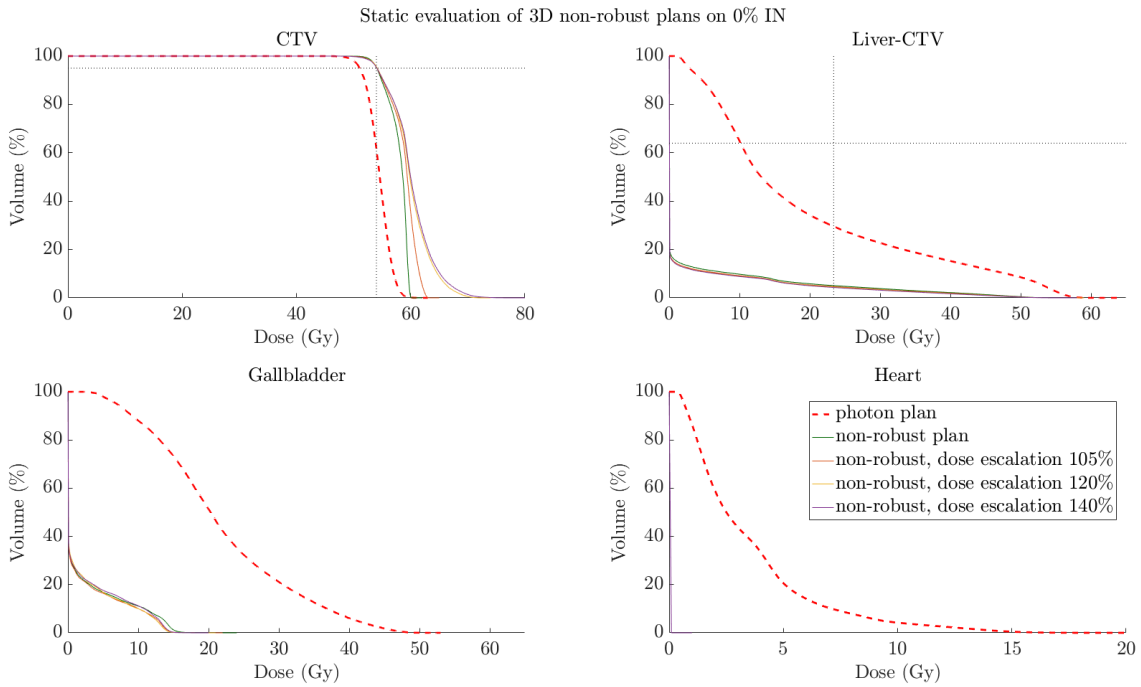

Figure 4.2: DVHs for 3D the non-robust treatment plans evaluated on the 0% IN phase. These plans just barely meet the clinical constraint for the CTV, as is indicated by the dotted lines.

As a preparation for the breath hold interplay analysis, the dose distributions are recomputed on the phases of 25% IN and 25% EX, see Figure 4.3. Here we immediately see a loss of CTV coverage on the recomputed phases and this will have a negative impact

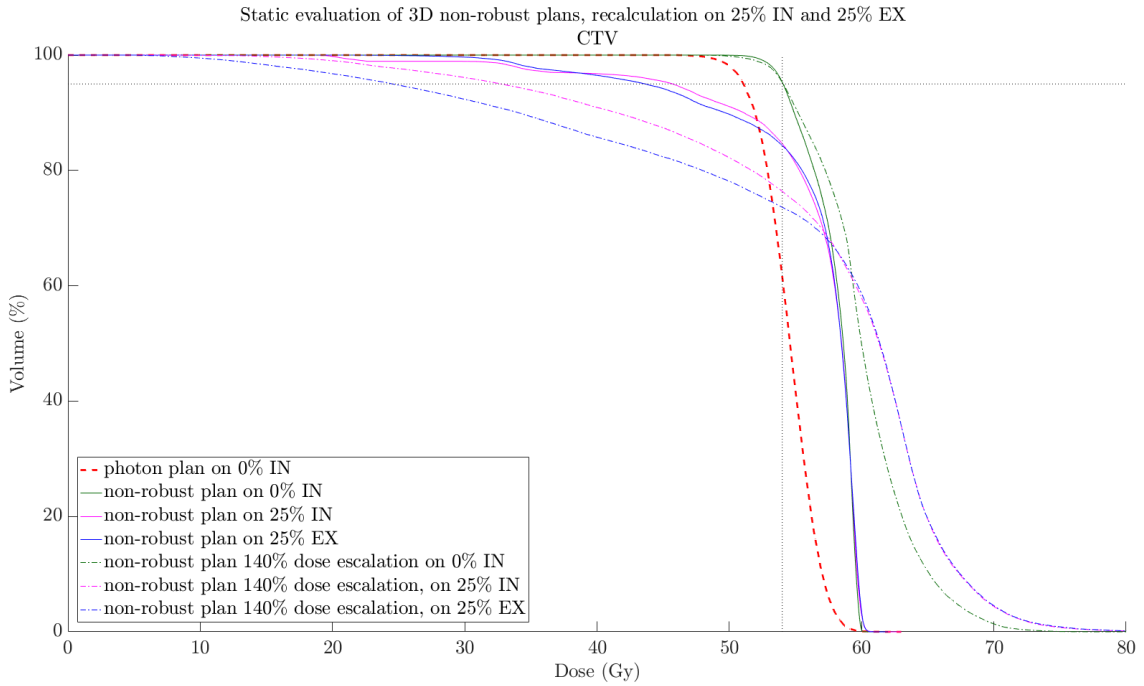

Figure 4.3: DVHs for the two of the examined non-robust plans on the 0% reference phase and also on the phases of 25% IN and 25% EX.

on the quality of the treatment delivery for the breath hold interplay analysis. This loss of CTV coverage is greater for the plan with 140% dose escalation than for the normal plan because the dose escalation plan has a sharper dose fall-off (penumbra) around the target volume, as a result of allowing higher inhomogeneities in the CTV dose, and can hence spare the surrounding tissue more. Sparing surrounding tissue, for this case, means that a higher weight will be put on the spots inside the target and that the spots around the CTV can be thrown away in the optimization because it yields a favorable result on the 0% IN phase. Not having spots around the CTV is however not that beneficial when studying target coverage in case of a small perturbation of the anatomy, as the recalculated dose distributions on the 25% IN and 25% EX phases are meant to illustrate. Notice that it is only the nominal scenario which is displayed here but that the CTV coverage is reduced even more when the other error scenarios are taken into account.

The results from 100 simulated treatments with the breath hold interplay analysis for the nominal scenario of the non-robust plan with 140% dose escalation can be seen in Figure 4.4. To the left in this figure, we can see that the CTV coverage has dropped to an unacceptably low value, independent of the fractionation scheme, and to the right in this figure we see that more than 50% of the target volume receives a dose which is higher than 60 Gy, this is a result which most likely stems both from allowing dose escalation and from the interplay effect. The clinical constraint on the CTV coverage is not met for this breath hold simulation of the nominal case. Studying the results for this treatment delivery simulation for one fraction for the error scenarios, we can see that the undershoot scenario performs worst on average, see Figure 4.5. As expected, the CTV coverage is reduced when studying the error scenarios in comparison with the nominal one and in this figure we can see that most error scenarios for the 3D non-robust proton therapy plan tends to have a CTV coverage which is similar to the one for the photon SBRT plan.

Figure 4.6 shows the results of the sensitivity analysis for the breath hold interplay

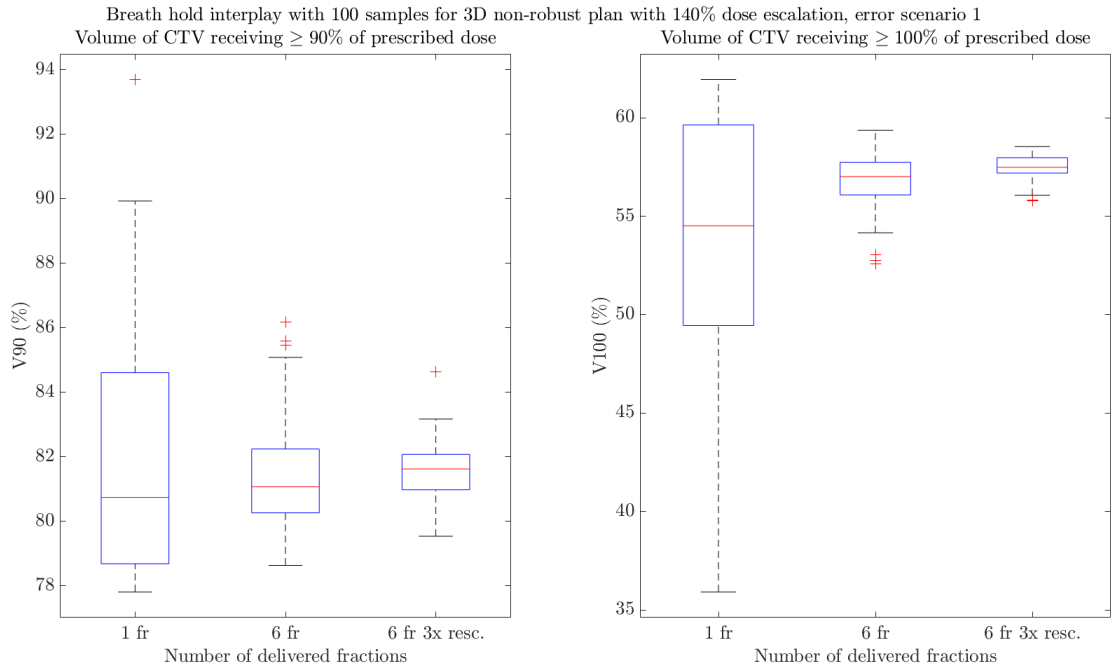

Figure 4.4: Boxplots showing statistics of 100 simulated treatments in breath hold for the nominal non-robust plan with 140% dose escalation for different fractionation schemes. The clinical constraint on the CTV coverage is not met.

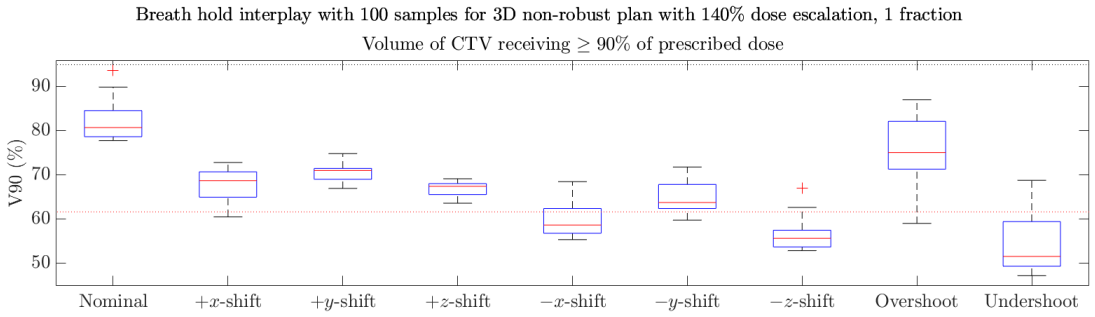

Figure 4.5: Boxplots showing statistics of the CTV coverage for 100 simulated treatments of one fraction in breath hold for the non-robust plan with 140% dose escalation. All the error scenarios are displayed separately in order to see which has the most negative impact on the treatment. The red dotted line visualizes the volume of the CTV receiving $\geq 90\%$ of the prescribed dose for the photon SBRT plan.

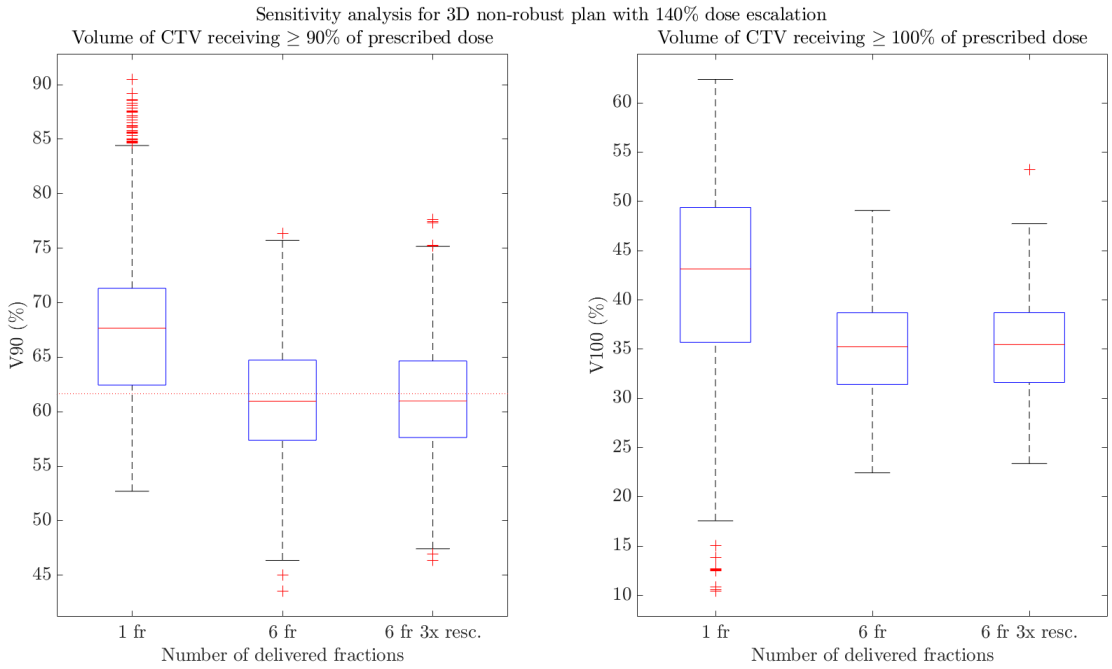

Figure 4.6: Boxplots showing statistics of the dose to the CTV for a sensitivity analysis of the breath hold interplay for the non-robust plan with 140% dose escalation for 1000 samples per fractionation scheme. The clinical constraints on the CTV coverage is not met.

with the non-robust plan with 140% dose escalation. As can be expected from studying the target coverage of all the separate error scenarios, this simulation also gives results which do not meet the clinical constraints. From these results of the 3D non-robust proton therapy plan with 140% dose escalation it is evident that this way of planning is too sensitive for treatment of moving targets since it is expected that the target position is not fully reproducible.

4.3 3D robust plan

The static evaluation of the DVHs for the 3D robust plan, on the 0% IN phase, for all the studied scenarios can be found in Figure 4.7. Here we can see that the clinical constraint on the CTV is met both for the nominal scenario and for all other error scenarios at the same time as this proton plan has superior OARs sparing in comparison to the photon SBRT plan. When this plan is recalculated on the 25% IN and 25% EX phases, for all error scenarios, we see that the clinical constraint is met in most, but not all, error scenarios, see Figure 4.8. Even though this robust plan does not meet the clinical constraint for all error scenarios on the phases of 25% IN and 25% EX, it already show a big improvement in comparison with the 3D non-robust plan were the coverage was significantly decreased even for the nominal cases, see Figure 4.3.

The results of the breath hold interplay simulation for the nominal case with 100 samples are showed in Figure 4.9. The clinical constraint on the CTV is met for all fractionation schemes in this case, but a big advantage in terms of reducing hot-spots can be seen when the treatment is delivered in more fractions and by the introduction of rescanning. This indicates that the interplay effect can be mitigated with rescanning for

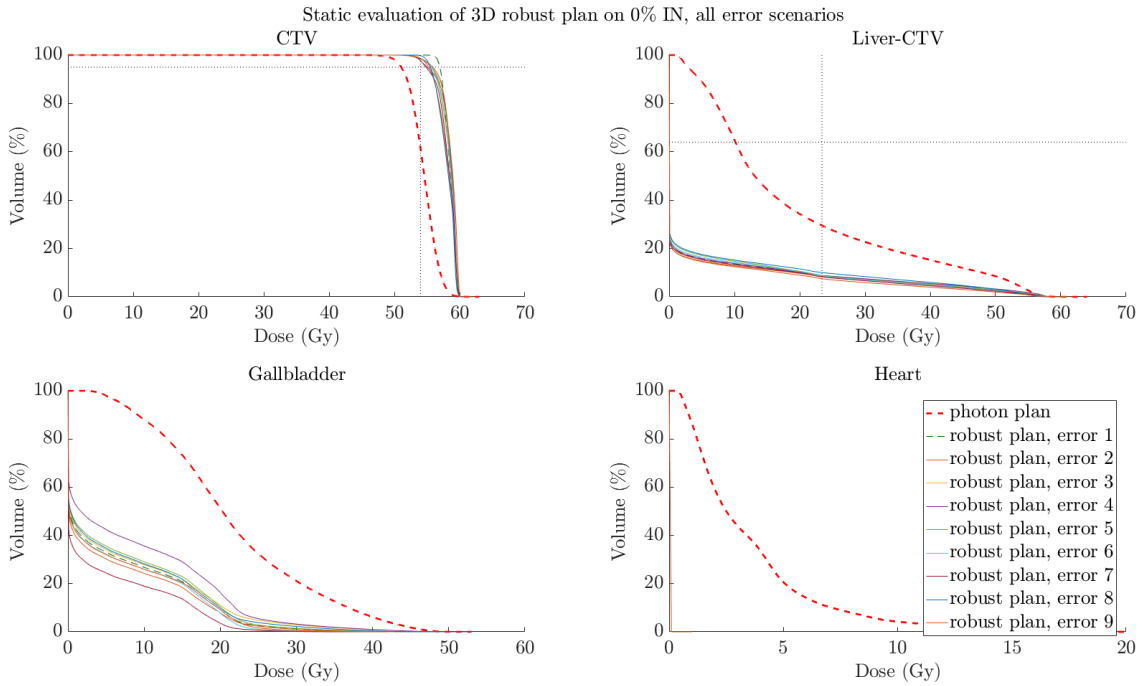

Figure 4.7: DVHs for the 3D robust treatment plan evaluated on the 0% IN phase for all error scenarios. The clinical constraints are met, for both the CTV and the liver-CTV, in all error scenarios. The robust proton plan has both better target coverage and better healthy tissue sparing than the photon plan.

this dose plan.

The doses to the CTV after the breath hold interplay simulation for all error scenarios are shown in Figure 4.10 for dose delivery in one fraction, in Figure 4.11 for dose delivery in six fractions and in Figure 4.12 for dose delivery in six fractions with three times rescanning. Comparing these three figures, we see that partitioning the dose in smaller pieces not only reduces the spread in the distributions but also mitigates the interplay effect. The result of this is that both hot- and cold-spots are reduced in the CTV with more complex fractionation scheme. It should here be noted that all treatment deliveries have insufficient CTV coverage for a shift of the patient in $-z$-direction with respect to the beam (error scenario 7). This shortcoming is a consequence of the way the breath interplay is simulated in itself and not a flaw in the treatment plan. The reason for this error scenario to have the greatest impact in the breath hold interplay is because the perturbation of the anatomy is also in the $-z$-direction, the phases of 25% IN and 25% EX being inferior to the 0% phase, and the robustness setting of this plan is not able to counteract the combination of these two disturbances together.

The results from the sensitivity analysis for the breath hold interplay simulation with the 3D robust plan are shown in Figure 4.13. These treatment simulations show a much better CTV coverage than the 3D non-robust plan with dose escalation, see Figure 4.6. This can be expected because of the good CTV coverage for the robust plan in the separate error scenarios, see Figure 4.7 and Figure 4.8. Note though, that only the treatment delivery in six fractions and in six fractions with three times rescanning meet the clinical constraint on the CTV (not taking the outliers into account). Also note that the simulated treatments converges towards the actually optimized plan with increasing the number of fractions and by introducing rescanning, see Figure 4.14.

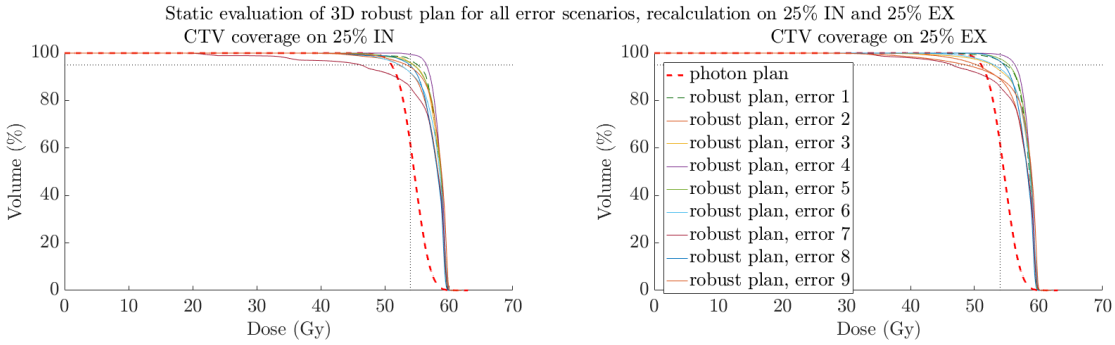

Figure 4.8: Dose coverage of the CTV when the 3D robust plan is recalculated on the phases of 25% IN and 25% EX. The clinical constraint is met for most scenarios and error scenario 4 even has better CTV coverage than the nominal case.

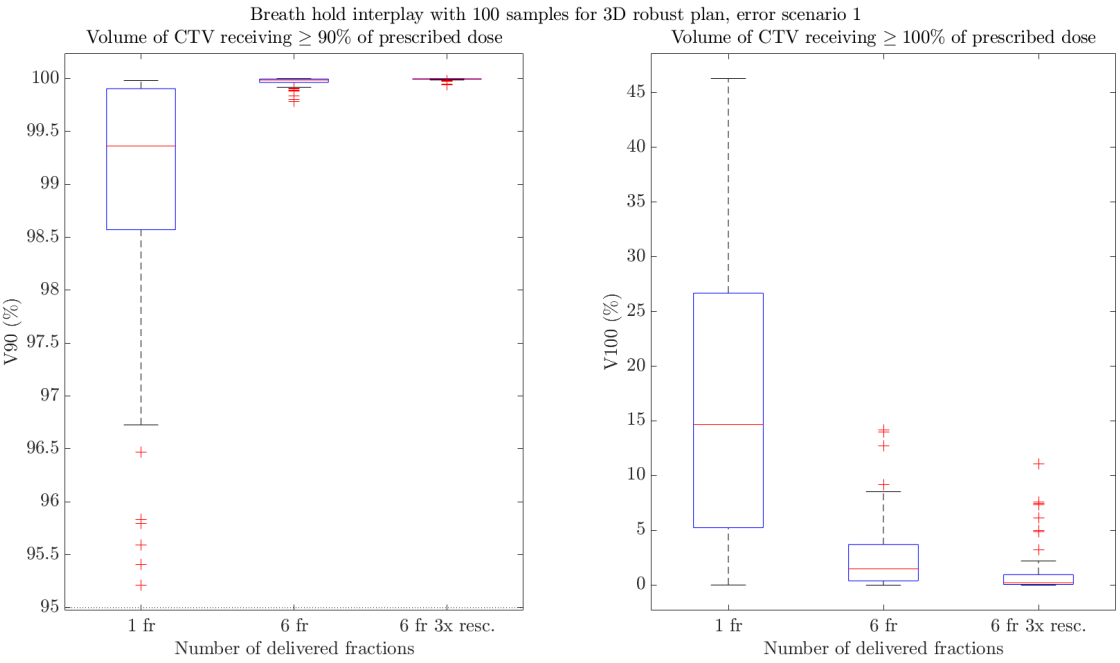

Figure 4.9: Results of the breath hold interplay simulation for the nominal scenario after 100 simulated treatments for different fractionation schemes. The clinical constraint on the CTV coverage is met for all the three ways of simulated treatment delivery.

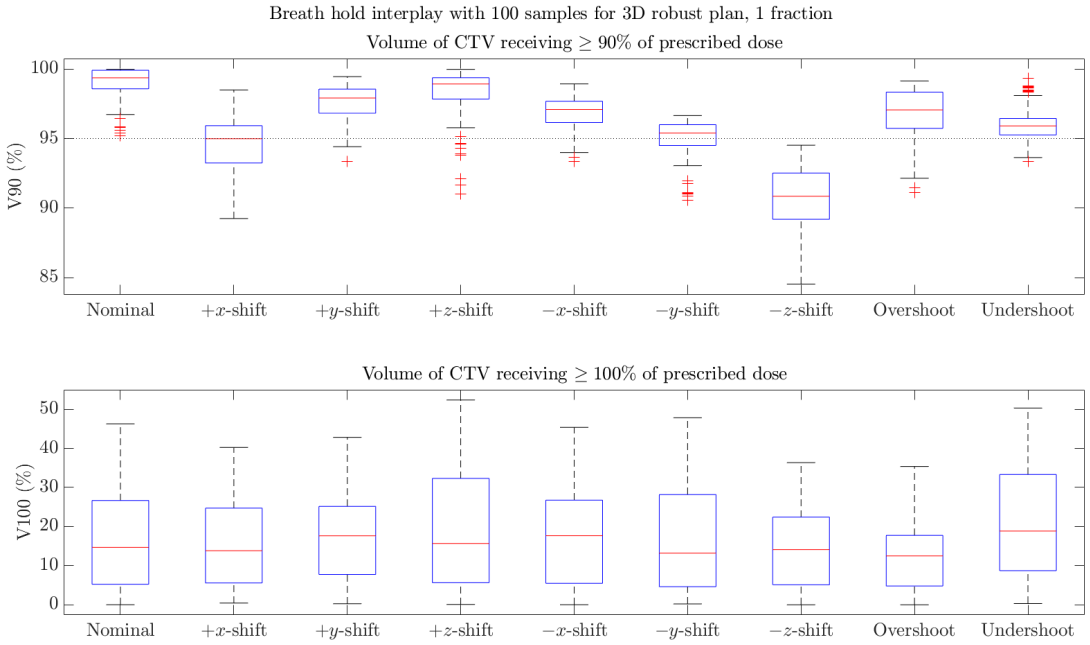

Figure 4.10: Boxplots showing statistics of the dose to the CTV, for every error scenario in the breath hold interplay, for 100 simulated treatment of one fraction. Only the nominal scenario met the clinical constraint for this type of treatment delivery.

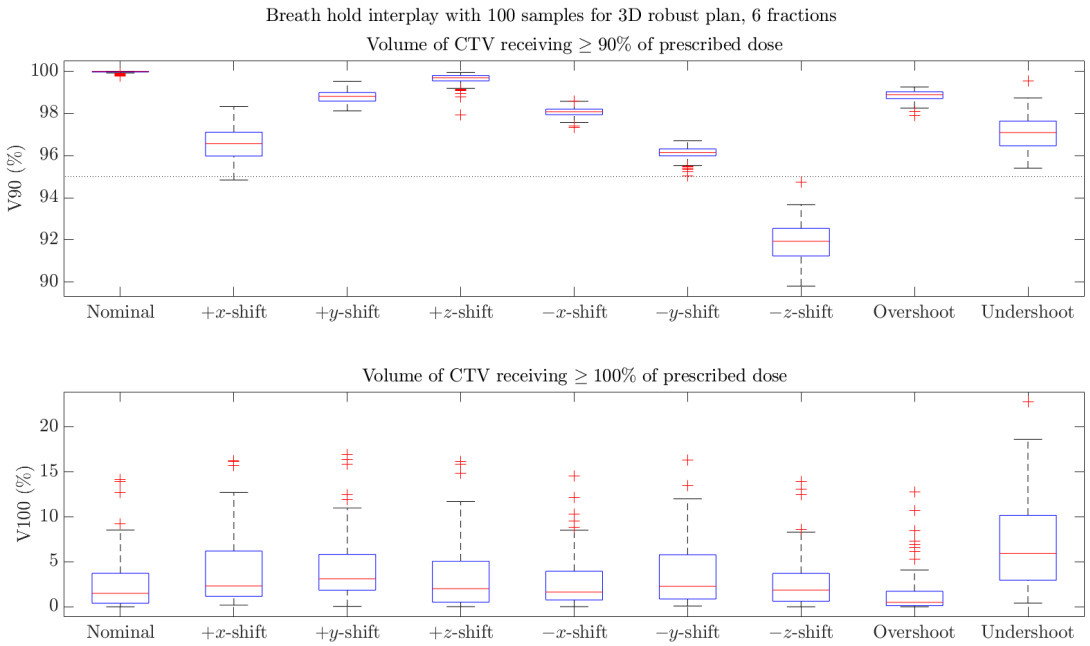

Figure 4.11: Boxplots showing statistics of the dose to the CTV, for every error scenario in the breath hold interplay, for 100 simulated treatment of six fractions. The clinical constraint is met in all error scenarios for all samples except for shift in $+x$-direction and shift in $-z$-direction.

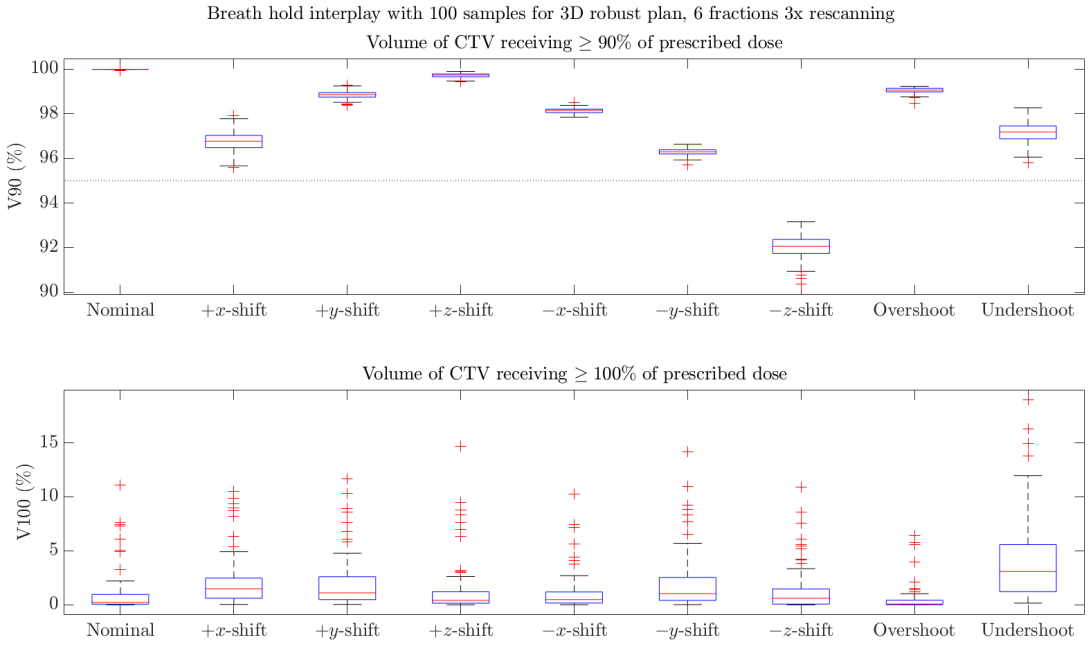

Figure 4.12: Boxplots showing statistics of the dose to the CTV, for every error scenario in the breath hold interplay, for 100 simulated treatment of six fractions with three times rescanning. The clinical constraint is met in all scenarios except for shift in $-z$-direction.

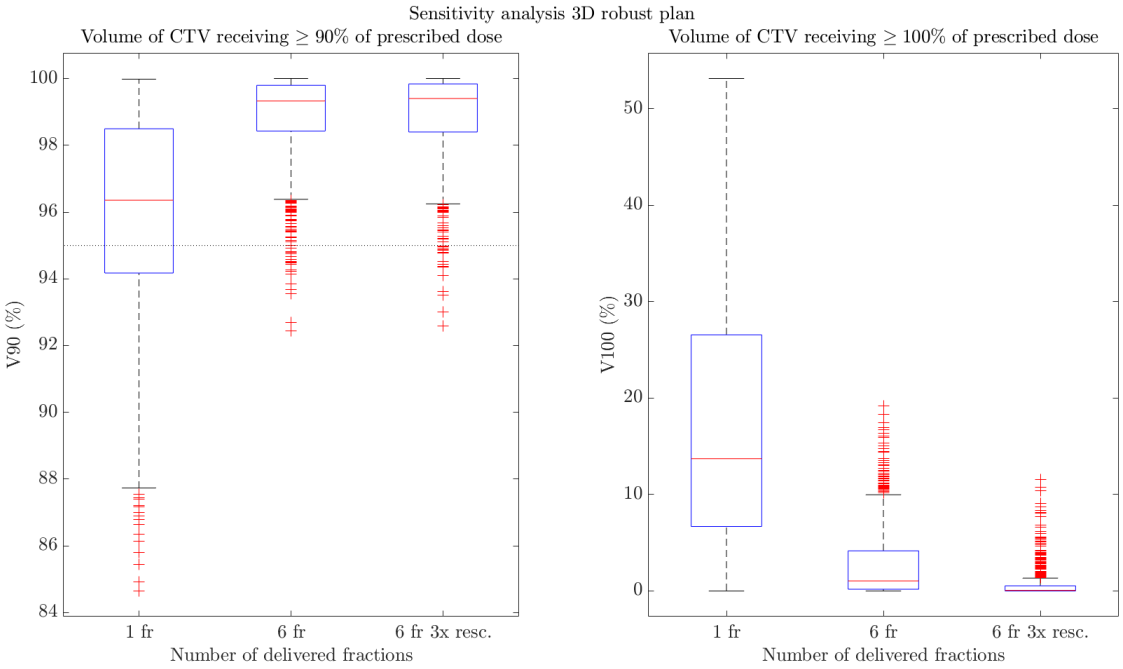

Figure 4.13: Boxplots showing statistics of the dose to the CTV for a sensitivity analysis of the breath hold interplay for the 3D robust plan for 1000 samples per fractionation scheme. All simulated treatments, which are not considered to be outliers, meet the clinical constraint when the treatment is delivered in six fractions or in six fractions with three times rescanning. Also note that the volume of the CTV which receives an overdosage is considerably decreased for these fractionation schemes in comparison to the one fraction delivery.

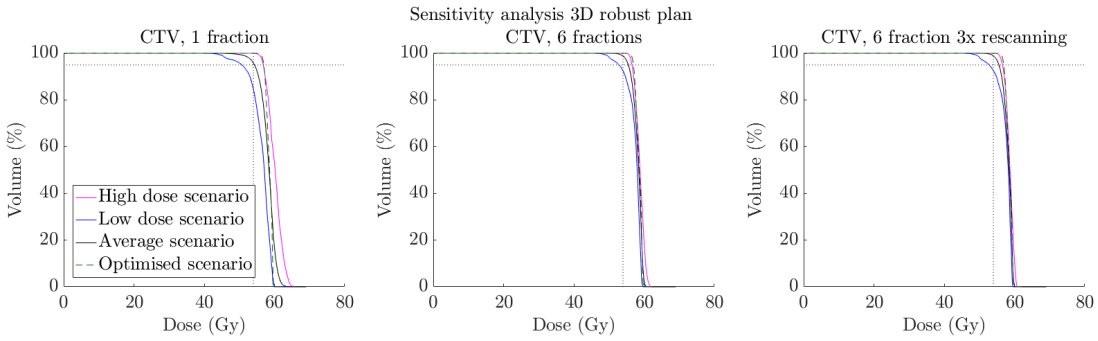

Figure 4.14: DVH curves showing the CTV coverage for different fractionation schemes in the sensitivity analysis. Note that with more fractions and rescans, all scenarios converges towards the optimized scenario.

4.4 4D non-robust plan on multiple CTs

The static CTV coverage of the 4D non-robust plan optimized on multiple phases can be seen in Figure 4.15. We can observe a clear reduction of the CTV coverage on the phases of 0% IN and 100% IN when comparing these to the 50% EX phase, and it is only the phase of 50% EX has a CTV coverage which is good enough to meet the clinical constraint. This 4D plan is meant to be delivered during free-breathing, and to have insufficient CTV coverage in the end-of-exhalation and end-of-inhalation phases is simply not clinically acceptable because it would yield a final dose distribution which is unsatisfactory. Taking this into account, it was decided that no further analysis would be carried out with this dose plan because of this sub-optimality in comparison to the other dose plans.

The reason for the poor performance of the multiple CT treatment plan optimization, for this patient, has not been established because of time limitations. A theory for this is though, that the movement of the target is to big for the studied case and that one set of spots (as the optimizer tries to find) is not able to cover the target in all positions without getting conflicting goals between the target and the OARs.

Efforts were made to also make 4D robust plan on multiple CTs, with the hope that this plan would have better target coverage in the phases of 0% IN and 100% IN. These efforts were in vain however, because using this method to plan robustly on this patient led to that fact that the optimization did not converge despite long planning time and many iterations.

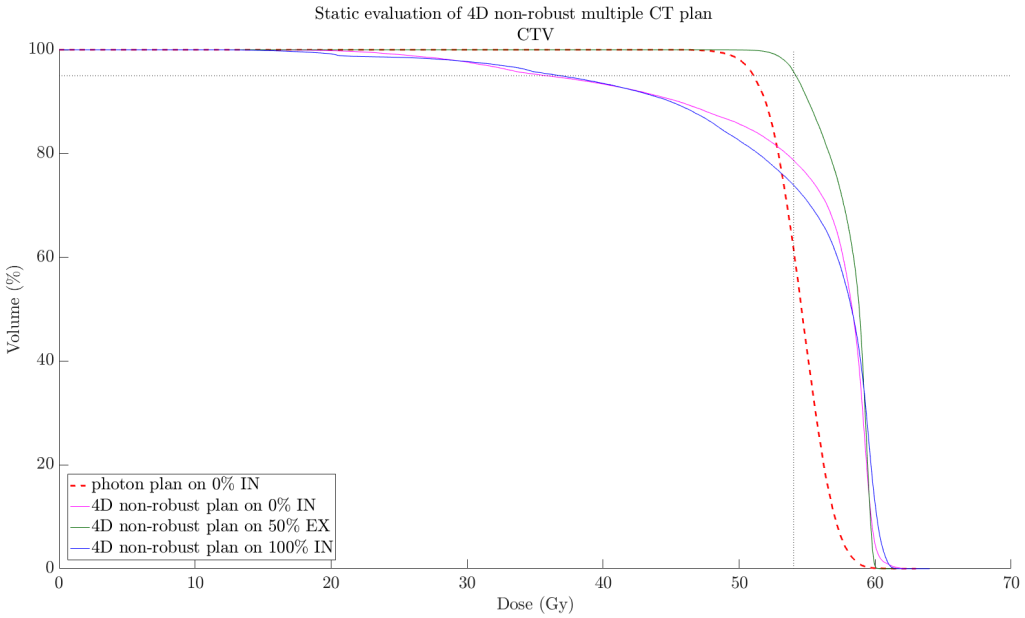

Figure 4.15: DVHs for CTV coverage of the 4D non-robust plan optimized on multiple phases. A distinct drop of the CTV coverage can be observed for the phases of 0% IN and 100% IN in comparison to the 50% EX phase.

4.5 4D robust ITV plan

The static evaluation of the DVHs for the 4D robust ITV plan can been seen in Figure 4.16. In this figure, we can evaluate the dose to the CTV, the liver-CTV, the gallbladder and to the heart for the five phases taken into account in the 4D interplay simulation. We can see that this dose plan meets the clinical constraints for both the CTV and the liver-CTV and that the CTV coverage for the proton plan is superior compared to the photon SBRT plan. The only obvious drawback with the 4D robust ITV plan in this comparison with the photon SBRT plan is that the proton plan gives a higher maximum dose to the liver-CTV. This result is however an inevitable feature of the ITV plan since the target volume is overlapping with the healthy tissue during the movement.

The results from the different error scenarios, studied separately, in 4D interplay simulations are shown in Figure 4.17, Figure 4.18 and Figure 4.19, for the different fractionation schemes, respectively. Comparing these three figures, we can see a clear positive impact of more fractions and rescans in terms of restoring dose homogeneity to the target and this applies for all error scenarios. Notice that the clinical constraint on the CTV coverage are not met for any scenario when the treatment is delivered in one fraction and that the opposite is true for dose delivery in six fractions (excluding the outliers) and in six fractions with three times rescanning. The volume of the target which is over-dosed is also reduced with an increasing number of "re-paintings". Also note that that this simulation does not show any noteworthy loss of CTV coverage for any of the error scenarios, as was the case for the 3D robust plan in the breath hold interplay simulation. This supports the hypothesis that it is not the 3D robust plan which is flawed but that it might not be optimal to perform the breath hold in the end-of-exhalation phase because it will lead to big disturbances for one particular error scenario.

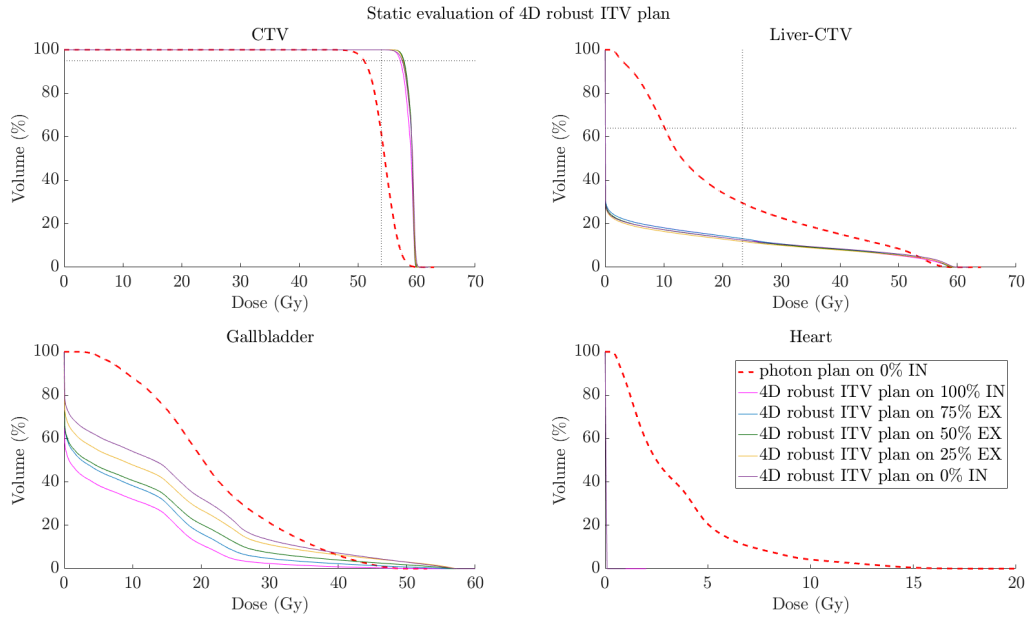

Figure 4.16: DVHs for the 4D robust treatment plan evaluated on all phases which are taken into account in the 4D interplay analysis. The clinical constraints for both the CTV and the liver-CTV are meet on all phases.

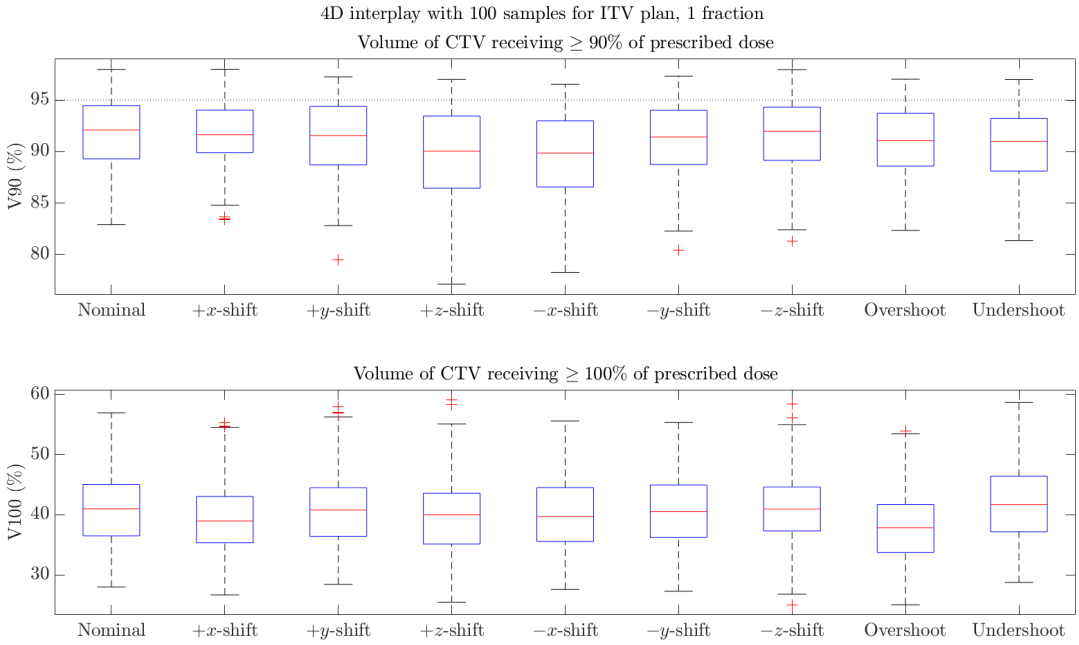

Figure 4.17: Boxplots showing statistics of the dose to the CTV for all considered error scenarios in the 4D interplay for treatment delivery in one fraction. The sample size was 100 simulated treatments for each error scenario. Non of these cases meet the clinical constraint on the CTV coverage.

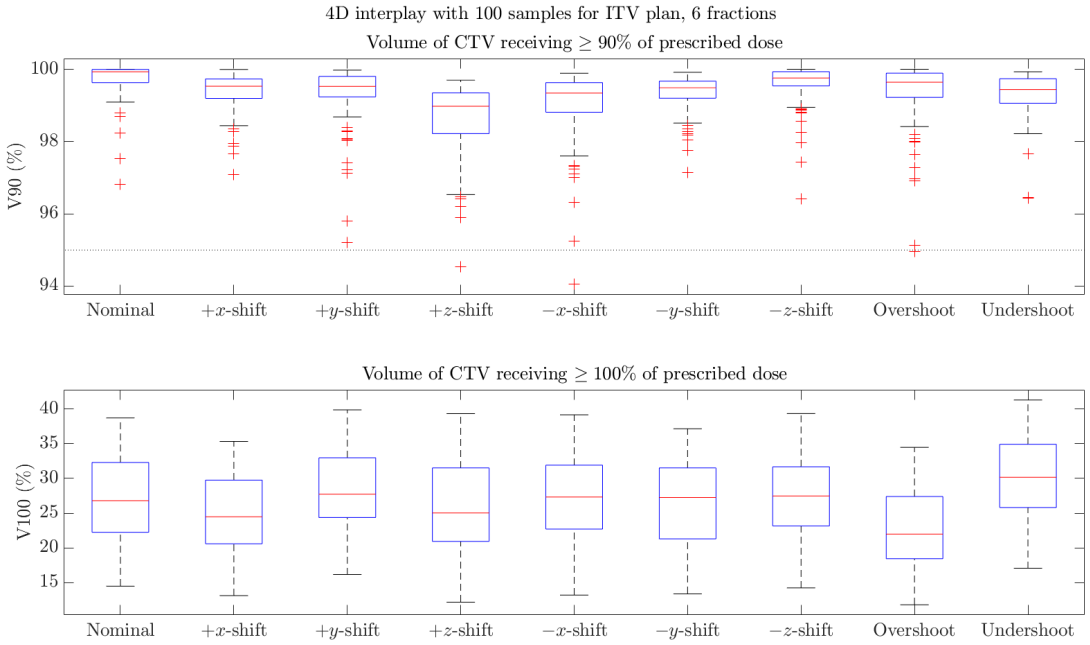

Figure 4.18: Boxplots showing statistics of the dose to the CTV for all considered error scenarios in the 4D interplay for treatment delivery in six fractions. The sample size was 100 simulated treatments for each error scenario. All cases meets the clinical constraint on the CTV coverage when excluding the outliers.

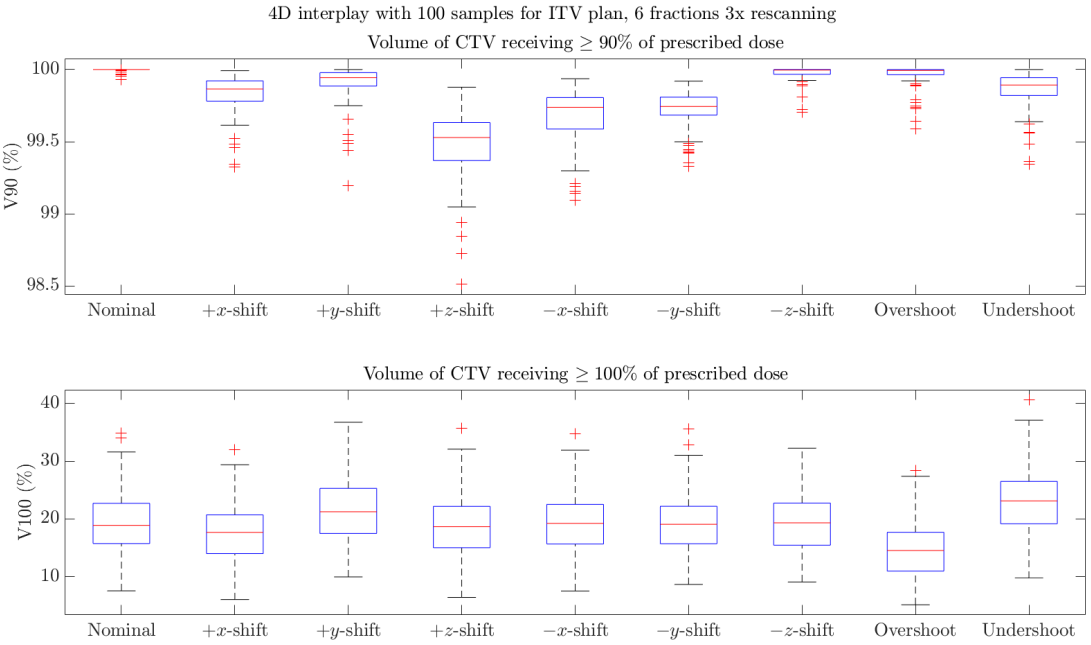

Figure 4.19: Boxplots showing statistics of the dose to the CTV for all considered error scenarios in the 4D interplay for treatment delivery in six fractions with three times rescanning. The sample size was 100 simulated treatments for each error scenario. All cases meets the clinical constraint on the CTV coverage.

Table 4.3: Number of dose spots, energy layers and the treatment time of each dose plan. The approximate treatment time for the different fractionation scheme is also presented. Note that time only includes the beam-on-time meaning that in the cases of the 3D plans, which would be delivered during breath hold, the total treatment time will be longer since the dose delivery is not continuous.

			Treatment time per fraction		
Plan	#spots	#energy layers	1 fraction	6 fractions	6 fr. 3x rescan.
3D non-robust	524	47	1.5 min	1.1 min	4.6 min
3D non-robust 105% dose escalation	458	44	1.5 min	1.1 min	4.4 min
3D non-robust 120% dose escalation	418	44	1.5 min	1.1 min	4.4 min
3D non-robust 140% dose escalation	378	44	1.4 min	1.0 min	4.4 min
3D robust	981	60	1.9 min	1.4 min	5.3 min
4D non-robust multi CT	471	48	1.5 min	1.1 min	4.6 min
4D robust ITV	1330	56	2.1 min	1.4 min	5.3 min

4.6 Comparison of different plans

Information about the treatment characteristics for the generated plans are to be found in Table 4.3. Here we can see that the result of allowing dose escalation is that fewer dose spots will be used in the treatment delivery because each spot inside the CTV itself, can have a higher weight. We can also see that more dose spots are required when planning robustly instead of non-robustly, some spots being placed not in but also around the target to ensure that the constraints are met in all the error scenarios. The treatment times for the dose plans in this table are approximate, but we can still notice that the 4D robust ITV plan, which has almost 40% more spots than the 3D robust plan, has roughly the same beam-on-time. This means that the dose delivery of the 4D robust ITV plan would be much faster than the 3D robust plan since it is meant to be delivered during free-breathing and not in breath hold.

A static DVHs comparison of three of the four examined treatment plan approaches is plotted in Figure 4.20. The plans examined in this figure are the photon plan, which is used as a baseline reference, the 3D non-robust plan with 140% dose escalation, the 3D robust plan and the 4D robust ITV plan. The 4D non-robust multi CT plan is excluded from this comparison since it does not fulfill the constraints on the optimized phases and can hence not be used in a clinical setting. In Figure 4.20 we can see that the two robust plans have better CTV coverage than the non-robust plan but that they also give more dose to the Liver-CTV. In comparison with the photon plan however, all proton plans give a significantly lower mean dose to the liver-CTV and the values for the normal tissue complication probability (NTCP) of the liver-CTV are also considerably reduced for the proton plans in this static evaluation, see Table 4.4.

In the simulation of the treatment delivery, it was only the 3D and the 4D robust treatment plans which had the potential of meeting the clinical constraints. Both these plans showed best results for the irradiation scheme of six fractions and three times rescanning, see Figure 4.12 and Figure 4.19 for simulation of 100 samples for each error scenario. Comparing these two figures, we can see that the 4D robust ITV plan gives a slightly better CTV coverage than the 3D robust plan but that it also tends to over-dose that target more.

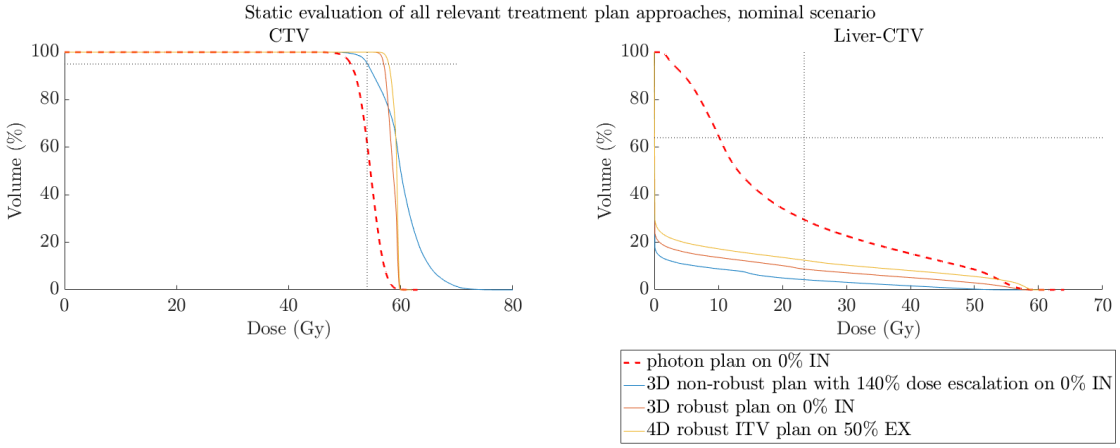

Figure 4.20: Static DVH comparison of the plans which meet the clinical constraints on the phases on which they are planned. All proton plans have a CTV coverage which is superior to the photon plan while they still provide better sparing of the liver-CTV.

Table 4.4: Treatment plan information from static evaluation. The photon and the 3D proton plans have been evaluated on the phase of 0% IN and the 4D proton plans on the 50% EX using Erasmus MatterhornRT. Notice that the maximum dose to the organs is evaluated in one voxel only.

Plan	Mean dose (Gy)		NTCP (%)	Max dose (Gy)	
	CTV	liver-CTV		gallbladder	heart
photon SBRT	54.5	17.2	2.93347	48.6	18.1
3D non-robust	57.8	2.9	1.28067×10^{-6}	23	0
3D non-robust 105% dose escalation	58.7	2.7	8.23202×10^{-7}	21.5	0
3D non-robust 120% dose escalation	59.9	2.6	6.51324×10^{-7}	20.1	0
3D non-robust 140% dose escalation	60.1	2.6	5.49656×10^{-7}	20.6	0
3D robust	58.5	4.8	2.78378×10^{-6}	45.6	0
4D non-robust multi CT	57.9	2.9	1.23826×10^{-6}	47	0
4D robust ITV	59.1	6.7	0.000151964	57.1	0

5

Discussion

Four different plan approaches, for the treatment of hepatocellular carcinoma (HCC) using intensity modulated proton therapy (IMPT), have been developed and evaluated in this project. Two of these plans are meant for treatment delivery in breath hold and two of them for treatment delivery during free-breathing. The 3D non-robust plan met the constraints in the static evaluation but in the simulation of treatment delivery, this plan does not yield good enough results to be clinically applicable. The 4D non-robust plan is not clinically relevant either because this plan only gave good target coverage on the intermediate 50% EX phase. To be clinically applicable in a 4D perspective, the treatment plan has to meet the CTV constraint during the full breathing cycle.

What is then left to investigate are the two robust plans. The robustness setting for the setup error for both robust plans was chosen to be 5 mm because the CTV to PTV margin in the photon plan was 5 mm. When studying the results from the breath hold interplay and the 4D interplay, for all the error scenarios separately, we can see that the impact of the interplay effect can be mitigated when introducing fractionation of the treatment and by applying rescanning, this result is in agreement with resembling studies found in literature [7, 19, 20]. This mitigation works very well for all scenarios included in this analysis except for a shift of the patient in $-z$-direction (error scenario 7) in the simulation of the breath hold interplay.

As mentioned before, the problem with a shift in $-z$-direction was consistently present in all results obtained from the breath hold interplay as it stems from an inherent problem from the modelling of this dose delivery technique, and is hence not depending on a weakness of the treatment plan. The root to the problem is that the breath hold simulation, performed in this project, is a worst case scenario for treatment delivery in breath hold. The reason for this is both because the two phases, on which the plan is not optimized on (25% IN and 25% EX), both are shifted in the inferior ($-z$) direction with respect to 0% IN and because these two phases are quite far from the reference phase if the lung volumes are compared. The fact that the anatomy is only shifted in one direction introduces the risk of missing the most inferior parts of the tumor completely, and one should take into account the approximately $\frac{2}{3}$ of the dose will be delivered to these shifted phases in the breath hold interplay analysis. In order to simulate this problem in a more realistic way, it would therefore be preferred to do the breath hold in, for example, the phase of 30% EX as it is proposed in [28]. The phase of 30% EX shows a good trade-off between reproducibility and motion during the breath hold and a breath hold in 30% EX is also easier to maintain than a breath hold in 0% IN. Besides this, it can also be assumed that reproducing a 30% EX breath hold would introduce position errors in both superior and inferior direction, and this would be advantageous in counteracting loss of CTV coverage illustrated when only a shift in $-z$-direction is introduced.

As might have been noticed by the reader when studying the dose-volume histograms (DVHs) in Chapter 4, is that the photon plan does not meet the clinical constraints on

the CTV coverage, which are stated in Table 3.1. The reason for this is probably that the dose constraints on the target could not be fulfilled without giving too high dose to the organs-at-risk. Even though this can be bewildering, the photon plan can still be used as a baseline scenario in the comparison with the proton plans and it only illustrates the benefit of using IMPT in treatment of HCC even more clearly.

6
Conclusion

The results from this study shows good prospects for the treatment of hepatocellular carcinoma (HCC) with intensity modulated proton therapy (IMPT) for dose delivery of robust plans in both breath hold and during free-breathing. The trade-off between the delivery of the 3D robust plan and the 4D robust ITV plan is treatment time versus the dose to the healthy liver. The 3D robust plan is able to spare more of the liver than the 4D robust plan, but the treatment time is expected to be considerably longer since it is delivered during breath hold. The choice of treatment approach hence depends on both the time available at the treatment facility and the acceptable liver dose. Note here that these conclusions are patient specific, since this study only included one patient, and more patient cases have to be evaluated in the future in order to be able to draw more general conclusions about treating HCC with IMPT.

Further recommendations for future research will shortly be described in list below;

- Investigate how to automate contour propagation on 4DCT datasets and examine how the accuracy of these contour influences the result of an interplay simulation.
- Study how to improve the quality of the CT transformations, made in Erasmus MatterhornRT, to get more truthful information about contributions to final dose distribution.
- Examine relevant values for setup uncertainties and determine if the choice for this value should be patient- or population-based.
- Look into the algorithm for the treatment planning on multiple CTs and try to draw conclusions about whether this patient specific case is infeasible for this planning approach, if the wish-list has to be improved or if there is an error in the algorithm.
- Study the reproducibility of breath holds further and examine if voluntary or assisted breath holds would be preferable.

Bibliography

[1] T. C. Ling, J. I. Kang, D. A. Bush, J. D. Slater, and G. Y. Yang, "Proton therapy for hepatocellular carcinoma," *Chinese Journal of Cancer Research*, vol. 24, no. 4, pp. 361–367, 2012. [Online]. Available: http://dx.doi.org/10.1007/s11670-012-0276-7

[2] A. M. Romero and A. Robert, "Stereotactic body radiation therapy for primary and metastatic liver tumors: From technological evolution to improved patient care," *Best Practice & Research Clinical Gastroenterology*, vol. 30, no. 4, pp. 603–616, 2016. [Online]. Available: http://dx.doi.org/10.1016/j.bpg.2016.06.003

[3] E. N. Marieb and K. Hoehn, *Human anatomy & physiology.* Pearson Education, 2007.

[4] C. Eccles, K. K. Brock, J.-P. Bissonnette, M. Hawkins, and L. A. Dawson, "Reproducibility of liver position using active breathing coordinator for liver cancer radiotherapy," *International Journal of Radiation Oncology* Biology* Physics*, vol. 64, no. 3, pp. 751–759, 2006. [Online]. Available: http://dx.doi.org/10.1016/j.ijrobp.2005.05.066

[5] L. A. Dawson, C. Eccles, and T. Craig, "Individualized image guided iso-NTCP based liver cancer SBRT," *Acta Oncologica*, vol. 45, no. 7, pp. 856–864, 2006. [Online]. Available: http://dx.doi.org/10.1080/0284186060093636

[6] J. Belghiti and R. Kianmanesh, "Surgical treatment of hepatocellular carcinoma," *HPB*, vol. 7, no. 1, pp. 42–49, 2005. [Online]. Available: https://doi.org/10.1080/13651820410024067

[7] G. Mondlane, M. Gubanski, P. A. Lind, T. Henry, A. Ureba, and A. Siegbahn, "Dosimetric comparison of plans for photon- or proton-beam based radiosurgery of liver metastases," *International Journal of Particle Therapy*, vol. 3, no. 2, pp. 277–284, 2016. [Online]. Available: http://dx.doi.org/10.14338/IJPT-16-00010.1

[8] H. Paganetti, *Proton Beam Therapy*, ser. 2399-2891. IOP Publishing, 2017. [Online]. Available: http://dx.doi.org/10.1088/978-0-7503-1370-4

[9] E. Podgorsak *et al.*, *Radiation Oncology Physics: A Handbook for Teachers and Students.* IAEA, 2005. [Online]. Available: http://dl4a.org/uploads/pdf/Pub1196_web.pdf

[10] J. E. Turner, *Atoms, radiation, and radiation protection.* John Wiley & Sons, 2008.

[11] INTERNATIONAL ATOMIC ENERGY AGENCY (IAEA), *Relative Biological Effectiveness in Ion Beam Therapy*, ser. Technical Reports Series. Vienna: INTERNATIONAL ATOMIC ENERGY AGENCY, 2008,

no. 461. [Online]. Available: http://www-pub.iaea.org/books/IAEABooks/7682/Relative-Biological-Effectiveness-in-Ion-Beam-Therapy

[12] H. Paganetti, "Relative biological effectiveness (RBE) values for proton beam therapy. Variations as a function of biological endpoint, dose, and linear energy transfer," *Physics in medicine and biology*, vol. 59, no. 22, p. R419, 2014.

[13] G. Giovannini, T. Böhlen, G. Cabal, J. Bauer, T. Tessonnier, K. Frey, J. Debus, A. Mairani, and K. Parodi, "Variable RBE in proton therapy: comparison of different model predictions and their influence on clinical-like scenarios," *Radiation Oncology*, vol. 11, no. 1, p. 68, 2016.

[14] M. Guckenberger, N. Andratschke, H. Alheit, R. Holy, C. Moustakis, U. Nestle, and O. Sauer, "Definition of stereotactic body radiotherapy," *Strahlentherapie und Onkologie*, vol. 190, no. 1, pp. 26–33, 2014. [Online]. Available: http://dx.doi.org/10.1007/s00066-013-0450-y

[15] N. G. Burnet, S. J. Thomas, K. E. Burton, and S. J. Jefferies, "Defining the tumour and target volumes for radiotherapy," *Cancer Imaging*, vol. 4, no. 2, pp. 153–161, 2004. [Online]. Available: http://dx.doi.org/10.1102/1470-7330.2004.0054

[16] International Commission on Radiation Units & Measurements, Inc. (ICRU), "Report 50," *Prescribing, recording and reporting photon beam therapy*, 1993.

[17] A.-C. Knopf and A. Lomax, "In vivo proton range verification: a review," *Physics in medicine and biology*, vol. 58, no. 15, p. R131, 2013.

[18] F. Albertini, E. Hug, and A. Lomax, "Is it necessary to plan with safety margins for actively scanned proton therapy?" *Physics in medicine and biology*, vol. 56, no. 14, p. 4399, 2011. [Online]. Available: http://dx.doi.org/10.1088/0031-9155/56/14/011

[19] Y. Zhang, I. Huth, M. Wegner, D. C. Weber, and A. J. Lomax, "An evaluation of rescanning technique for liver tumour treatments using a commercial PBS proton therapy system," *Radiotherapy and Oncology*, vol. 121, no. 2, pp. 281–287, 2016. [Online]. Available: http://doi.org/10.1016/j.radonc.2016.09.011

[20] Y. Zhang, D. Boye, C. Tanner, A. Lomax, and A. Knopf, "Respiratory liver motion estimation and its effect on scanned proton beam therapy," *Physics in medicine and biology*, vol. 57, no. 7, p. 1779, 2012. [Online]. Available: http://dx.doi.org/10.1088/0031-9155/57/7/1779

[21] S. Lang and O. Riesterer. Modern Techniques in Radiation Oncology. Accessed 2017-05-29. [Online]. Available: http://www.sps.ch/en/articles/progresses/modern-techniques-in-radiation-oncology-36/

[22] S. Breedveld, *Towards Automated Treatment Planning in Radiotherapy: A Mathematical Approach to Automated and Integrated Multi-Criterial Optimization of Beam Angles and IMRT Fluence Profiles*, 2013.

[23] S. van de Water, A. Kraan, S. Breedveld, W. Schillemans, D. Teguh, H. Kooy, T. Madden, B. Heijmen, and M. Hoogeman, "Improved efficiency of multi-criteria impt treatment planning using iterative resampling of randomly placed pencil beams," *Physics in medicine and biology*, vol. 58, no. 19, p. 6969, 2013. [Online]. Available: https://doi.org/10.1088/0031-9155/58/19/6969

[24] L. A. Dawson, D. Normolle, J. M. Balter, C. J. McGinn, T. S. Lawrence, and R. K. Ten Haken, "Analysis of radiation-induced liver disease using the Lyman NTCP model," *International Journal of Radiation Oncology* Biology* Physics*, vol. 53, no. 4, pp. 810–821, 2002. [Online]. Available: http://dx.doi.org/10.1016/S0360-3016(02)02846-8

[25] A. Méndez Romero, "Transarterial Chemoembolization with Drug-Eluting Beads (standard arm) versus Stereotactic Body Radiation Therapy (experimental arm) for hepatocellular carcinoma: A multicenter randomized phase II trial 'The TRENDY trial', protocol v.1.3," 2016, Department of Radiation Oncology, Erasmus MC Cancer Institute, unpublished clinical trial protocol NL51318.078.14 / TRENDY.

[26] J. Ehrhardt, C. Lorenz *et al.*, *4D modeling and estimation of respiratory motion for radiation therapy.* Springer, 2013.

[27] E. D. Brandner, A. Wu, H. Chen, D. Heron, S. Kalnicki, K. Komanduri, K. Gerszten, S. Burton, I. Ahmed, and Z. Shou, "Abdominal organ motion measured using 4d ct," *International Journal of Radiation Oncology* Biology* Physics*, vol. 65, no. 2, pp. 554–560, 2006. [Online]. Available: http://dx.doi.org/10.1016/j.ijrobp.2005.12.042

[28] E. Lens, O. J. Gurney-Champion, D. R. Tekelenburg, Z. van Kesteren, M. J. Parkes, G. van Tienhoven, A. J. Nederveen, A. van der Horst, and A. Bel, "Abdominal organ motion during inhalation and exhalation breath-holds: pancreatic motion at different lung volumes compared," *Radiotherapy and Oncology*, vol. 121, no. 2, pp. 268–275, 2016. [Online]. Available: http://dx.doi.org/10.1016/j.radonc.2016.09.012